The Journal of Physiology

A common cause for nystagmus in different congenital stationary night blindness mouse models

Maj-Britt Hölzel[1], Wouter Kamermans[1], Beerend H. J. Winkelman[1,2], Marcus H. C. Howlett[1], Chris I. De Zeeuw[1,2] and Maarten Kamermans[1,3]

[1] *Netherlands Institute for Neuroscience Amsterdam, Amsterdam, the Netherlands*
[2] *Department of Neuroscience, Erasmus MC, Rotterdam, the Netherlands*
[3] *Department of Biomedical Physics, Academic Medical Center, University of Amsterdam, Amsterdam, the Netherlands*

Handling Editors: Richard Carson & Karin Dedek

The peer review history is available in the Supporting Information section of this article (https://doi.org/10.1113/JP284965#support-information-section).

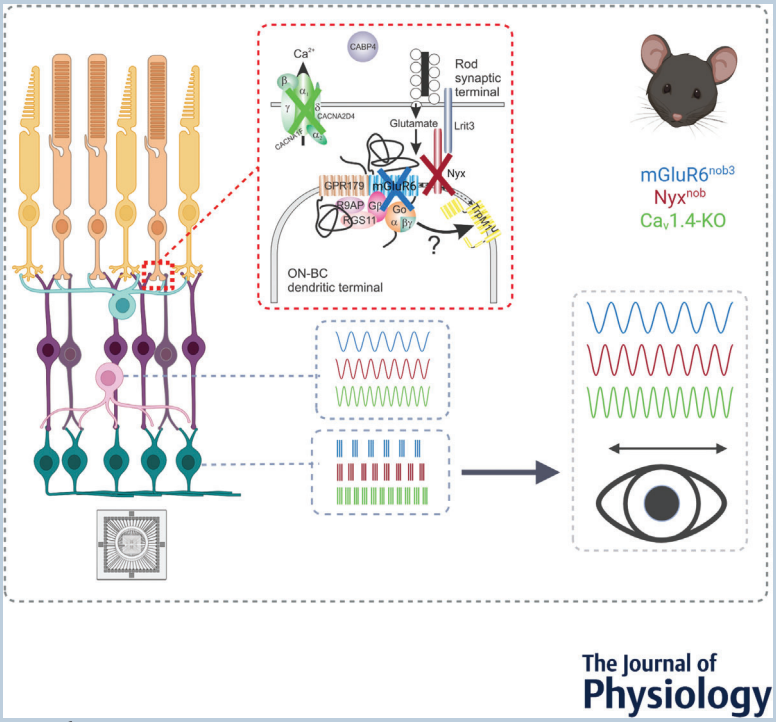

Abstract In *Nyx*^{nob} mice, a model for congenital nystagmus associated with congenital stationary night blindness (CSNB), synchronous oscillating retinal ganglion cells (RGCs) lead to oscillatory eye movements, i.e. nystagmus. Given the specific expression of *mGluR6* and *Ca$_v$1.4* in the photoreceptor to bipolar cell synapses, as well as their clinical association with CSNB, we hypothesize that *Grm6*^{nob3} and *Ca$_v$1.4-KO* mutants show, like the *Nyx*^{nob} mouse, oscillations in both their RGC activity and eye movements. Using multi-electrode array recordings of RGCs and measurements of the eye movements, we demonstrate that *Grm6*^{nob3} and *Ca$_v$1.4-KO* mice also show oscillations of

M. Hölzel and W. Kamermans shared first authorship.

This article was first published as a preprint. Hölzel M-B, Winkelman BHJ, Howlett MHC, Kamermans W, De Zeeuw CI, Kamermans M. 2023. A Common Cause for Nystagmus in Different Congenital Stationary Night Blindness Mouse Models. bioRxiv. https://doi.org/10.1101/2023.04.24.538135

DOI: 10.1113/JP284965

their RGCs as well as a nystagmus. Interestingly, the preferred frequencies of RGC activity as well as the eye movement oscillations of the *Grm6*^{nob3}, *Ca*$_v$*1.4-KO* and *Nyx*^{nob} mice differ among mutants, but the neuronal activity and eye movement behaviour within a strain remain aligned in the same frequency domain. Model simulations indicate that mutations affecting the photoreceptor–bipolar cell synapse can form a common cause of the nystagmus of CSNB by driving oscillations in RGCs via A_{II} amacrine cells.

(Received 1 May 2023; accepted after revision 22 September 2023; first published online 23 October 2023)
Corresponding author M. Kamermans: Netherlands Institute for Neuroscience Amsterdam, Amsterdam, the Netherlands. Email: m.kamermans@nin.knaw.nl

Abstract figure legend Mechanism underlying congenital nystagmus in CSNB mouse models. Mutations in genes encoding for proteins in the photoreceptor to ON-bipolar cell synapse lead to a more depolarized membrane potential of the AII amacrine cell, which in turn starts to intrinsically oscillate. The oscillations are forwarded to the retinal ganglion cells that start oscillating as well. This includes the ON-direction selective ganglion cells which measure global motion of an image. They send this oscillatory signal to the accessory optic system, where compensatory, oscillatory eye movementsare induced; the nystagmus.

Key points

- In *Nyx*^{nob} mice, a model for congenital nystagmus associated with congenital stationary night blindness (CSNB), their oscillatory eye movements (i.e. nystagmus) are caused by synchronous oscillating retinal ganglion cells.
- Here we show that the same mechanism applies for two other CSNB mouse models – *Grm6*^{nob3} and *Ca*$_v$*1.4-KO* mice.
- We propose that the retinal ganglion cell oscillations originate in the A_{II} amacrine cells.
- Model simulations show that by only changing the input to ON-bipolar cells, all phenotypical differences between the various genetic mouse models can be reproduced.

Introduction

Patients with congenital stationary night blindness (CSNB) often have congenital nystagmus as well (Bijveld et al., 2013; Pieh et al., 2008). These involuntary, oscillating eye movements occur shortly after birth and vary from pendular to jerk nystagmus (Optican & Zee, 1984; Pieh et al., 2008). Previously, we reported that *Nyx*^{nob} mice, a CSNB mouse model (Gregg et al., 2003; Pardue et al., 1998), have a pendular nystagmus that results from the oscillatory output of retinal ganglion cells (RGCs; Winkelman et al., 2019). This oscillatory firing of RGCs appears to be driven by A_{II} amacrine cells (A_{II} ACs), which are probably depolarized outside of their normal working range due to the lack of ON-bipolar cell (ON-BC) input (Winkelman et al., 2019).

The photoreceptor to ON-BC synapse is a highly specialized metabotropic glutamatergic synapse (Fig. 1). Depolarization of a photoreceptor opens its $Ca_v1.4$ calcium channels and the resulting influx of Ca^{2+} into its synaptic terminal ultimately leads to glutamate release (Schmitz & Witkovsky, 1997). The released glutamate

Maj-Britt Hölzel obtained both her Bachelor of Science in Biology (major) and Chemistry (minor) and her Master of Science in Biology at the Carl von Ossietzky University Oldenburg (Germany), where she discovered her passion for the retina and electrophysiology. She is now a PhD student in the Retinal Signal Processing department at the Netherlands Institute for Neuroscience in Amsterdam, where she investigates the retinal origin of congenital nystagmus. **Wouter Kamermans** obtained his bachelor's degree in physics at Fontys University of Applied Sciences. He then pursued a master's degree in computational modelling and control system engineering at HAN University of Applied Sciences, where he further developed his interest in complex control systems and discovered a passion for control systems in biological contexts. Currently, he is working towards a PhD in neuroscience at the Netherlands Institute for Neuroscience, where he is studying the control systems of eye movements.

diffuses across the synaptic cleft and binds to the post-synaptic metabotropic glutamate receptors (mGluR6; Masu et al., 1995). Activation of this receptor triggers a G-protein-coupled cascade, which leads to the closure of TRPM1 channels resulting in ON-BC hyperpolarization (Morgans et al., 2009; Shen et al., 2009). The function of this synapse depends crucially on the close interaction of all the synaptic proteins involved.

Mutations of the various proteins involved in this synapse will each affect the ON-BC differently. Post-synaptically, there are varying degrees of interdependency between the elements of the signalling cascade. For instance, elimination of mGluR6 disrupts both the expression levels and subcellular targeting of most signalling molecules so far examined. By contrast, when the scaffolding protein nyctalopin is lost, TRPM1 is no longer correctly trafficked and localized to the dendritic tips but other elements of the signalling cascade remain unaffected (Cao et al., 2009, 2011; Gregg et al., 2007, 2014; Martemyanov & Sampath, 2017; Pardue et al., 1998; Pearring et al., 2011; Ray et al., 2014). In *Grm6*^{nob3} mice (Maddox et al., 2008), the mGluR6 receptors are not functional, which leads to open TRPM1 channels depolarization of the ON-BCs (Ishii et al., 2009; Koike et al., 2010; O'Connor et al., 2006; Tagawa et al., 1999). On the other hand, mutations that affect the $Ca_v1.4$ channel impair presynaptic signalling while leaving post-synaptic signalling intact (Specht et al., 2009), photoreceptors do not release glutamate and, as under light conditions, the mGluR6 receptor is not activated and the TRPM1 channels are open. This leads to a depolarization of the ON-BCs. These different conditions will probably lead to different membrane potentials of the ON-BC and possibly to slightly different phenotypes of CSNB.

There are several CSNB mouse models, each with a different photoreceptor to ON-BC synapse-specific protein mutated (Zeitz et al., 2015). As mutations in each of these different proteins probably affect the ON-BC differently, it is possible that each mutation presents with a phenotypically distinct nystagmus. To test this idea, we studied eye movements and RGC activity in two CSNB mouse models: *$Ca_v1.4$-KO* and *Grm6*^{nob3} mice and compared the results with those of *Nyx*^{nob} mice. We found that all CSNB mouse models had a disturbed optokinetic response (OKR), nystagmus and oscillating RGCs. However, each mouse model displayed phenotypically distinct features including different eye movements and RGC oscillation frequencies. Furthermore, we found that flashes of light at various intensities, which should polarize the A_{II} ACs to differing degrees, changed the oscillation frequency of *Nyx*^{nob} RGCs. Model simulations show that these phenotypical changes can indeed be generated by exclusively changing the ON-BC input.

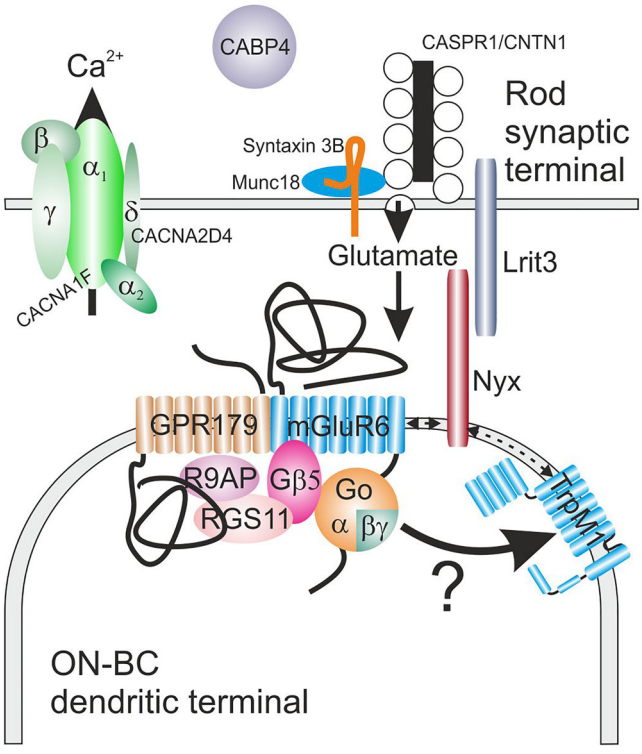

Figure 1.
Schematic overview of the photoreceptor to ON-bipolar cell synapse

Material and methods

Animals

All animal experiments were carried out under the responsibility of the ethical committee of the Royal Netherlands Academy of Arts and Sciences (KNAW) acting in accordance with the European Communities Council Directive of 22 September 2010 (2010/63/EU). The experiments were performed under licence numbers AVD-801002016517 and AVD-80100202115698, issued by the Central Committee for Animal Experiments of the Netherlands.

Grm6^{nob3} and *Nyx*^{nob} mice were obtained from the McCall lab (University of Louisville, Louisville, KY, USA) and *$Ca_v1.4$-KO* mice from the Koschak lab (University of Innsbruck, Innsbruck, Austria). All mice were in a C57BL/6JRj background either with or without a GFP label on ON-dsRGCs coding for upward motion (SPIG1^{+} mice; Yonehara et al., 2009). Since the Nyx mutation is X-linked, only male mice in the age range 5–71 weeks were used for the experiments. Room lights were timed on a 12/12 h light–dark schedule, and experiments took place during daytime. Mice had *ad libitum* access to food and water.

Eye movement recordings

Surgical preparation. Before the start of experiments, adult animals were equipped with a head-fixation pedestal, an anodized aluminium bit with an integrated magnet, attached to the parietal and frontal bones of the skull using dental cement (Super Bond C&B, Sun Medical, Japan). Surgery was performed under general isoflurane/O_2 and topical anaesthesia (bupivacaine). Analgesia was offered by subcutaneous injection of carprofen (5 mg/kg). The recovery time was at least 2 days after pedestal surgery. During experiments, the animal was placed head-fixed in the experimental setup using a custom-made adapter, which allowed panoramic vision.

Optokinetic stimulus setup. Optokinetic stimuli were displayed on two Benq XL2420t high-performance monitors (120 fps, gamma-1.745) that were placed in V-formation around the animal. The closest distance between the screen surface and the mouse head was 16.5 cm. Screen dimensions were 56.9 × 33.8 cm (combined field of view: 240 × 50°). For measurements in darkness, the displays were switched off. Mickelson contrast of the grayscale grating stimuli was 99.67%. Visual stimuli consisted of sine wave gratings (mean luminance: 71.6 cd/m^2) and homogeneous grayscale images (mean luminance: 71.6 cd/m^2).

Eye movement recordings. Eye movements were recorded using an infrared video tracking system (JAI RM-6740CL monochrome CCD camera, 200 fps, 850 nm illumination). Pilocarpine (2%) eye drops were used to reduce pupil size in case the pupil was too large to track. Online image analysis extracted the location of pupil edges and corneal light reflections from each frame using custom-built software for LabVIEW (National Instruments, Austin, TX, USA). Eye position was computed from the relative distance between pupil centre and corneal reflections of the infrared LEDs (Stahl et al., 2006) and pupil size (Stahl, 2002; Stahl et al., 2000). Epochs containing saccades, eye blinks and motion artefacts were excluded from analysis. Eye velocity was smoothed using a Gaussian smoothing kernel with an SD of 7.5 ms (25 Hz cut-off). All OKR measurements were done monocularly, during which the contralateral eye was covered by a miniature blackout cap.

Analysis of eye movement recordings. The power spectral density (PSD) was computed from angular eye velocity using Welch's method with a 4 s window length, 75% overlap between windows and a Hann window function.

Multielectrode RGC recordings

Retinal dissection. Multielectrode RGC recordings were performed as described previously (Hölzel et al., 2022; Winkelman et al., 2019). After 60–75 min of dark adaptation, mice were sedated using a mixture of CO_2/O_2 and ultimately killed by cervical dislocation. All procedures were carried out under dim red light. The eyes were extracted from the eye socket and placed in room temperature Ames' medium (Sigma-Aldrich, St Louis, MO, USA). Next, the cornea and lens were removed by making an insertion around the ora serrata using fine spring scissors. As much vitreous humour as possible as well as the sclera were removed using fine forceps. Four small insertions were made and the retina was flat mounted on a filter paper annulus (1 mm inner radius; 0.8 μm hydrophilic MCE MF-Millipore membrane filter, Merck Millipore, Tullagreen, Ireland). The retina was then mounted photoreceptor cell side up on a perforated 60-electrode MEA chip (60pMEA200/30iR-Ti, Multichannel systems, Reutlingen, Germany) in a recording chamber mounted on a Nikon Optiphot-2 upright microscope and viewed under infrared light with an Olympus 2× objective and video camera (Abus TVCC 20530). During the experiment the retina was continuously superfused with Ames' medium gassed with a mixture of O_2 and CO_2 at a pH of 7.4 and a temperature of 35–36°C at a flow rate of 1.5 ml/min. Before the recording started, an acclimatization period in the dark for 15 min was given to ensure stable recordings.

Data acquisition. The extracellular RGC activity was acquired using MC rack (Multichannel systems) at a sampling frequency of 25 kHz. The data were then zero-phase bandpass filtered (250–6250 Hz) with a fourth-order Butterworth filter in Matlab (Mathworks, Natick, MA, USA). Subsequently the spiking activity was sorted manually into single unit activity using the Plexon offline sorter (Plexon, Dallas, TX, USA) based on the first two principal components *versus* time. For the extraction of spikes from the background, a spike detection amplitude threshold of $>4\sigma_n$ was used as criteria. Here, σ_n is defined as an estimation of the standard deviation of background noise and x is the bandpass-filtered signal (Quiroga et al., 2004):

$$\sigma_n = median\left(\frac{|x|}{0.6745}\right)$$

Optical stimulator. Full field white light flashes were generated using Psychophysics Toolbox Version 3 (Brainard, 1997) and presented to the photoreceptor side of the retina with a custom-modified DLP projector (for details of modification see Winkelman et al., 2019; Light Crafter 4500, Wintech, Carlsbad, CA, USA). For wild-type (WT),

Nyx^{nob} and *Ca*$_v$*1.4-KO* retinas, the full field light flash had a duration of 500 ms. For *Grm6*^{nob3} mice, the flash duration was extended to 2000 ms to accommodate for the lower RGC oscillatory frequencies present in this mouse model. In all cases the light flash was preceded by a 500 ms period of darkness and followed by a 1000 ms period of darkness and the stimulus was repeated 100 times. White light stimuli consisted of equal quantal output of the red (625 nm), green (530 nm) and blue (455 nm) LEDs. The maximal light intensity was 8.60 10^{19} quanta/m^2/s. When studying the effect of different light intensities on the *Nyx*^{nob} RGC oscillation frequency, two light intensities were used: 9.02×10^{18} and 8.60×10^{19} quanta/m^2/s.

Data analysis. To identify spontaneous oscillatory RGC activity, the firing activity in the dark was recorded for a period of at least 15 min. For each cell the activity was binned in 1 ms bins, and then divided into 5 s non-overlapping epochs. Each epoch was baseline subtracted and the autocorrelation and PSD determined. Based on these data the average autocorrelation and Welch's PSD were calculated for each cell. The RGCs of one of the five *Ca*$_v$*1.4-KO* retinas oscillated at much lower frequencies than the other four and was therefore excluded from the analysis. Mean light responses were calculated over the 100 stimulus repetition for each cell. Five hundred milliseconds of the mean light response of each cell that occurred after 50 ms after the light onset was zero padded to 2 s and used to calculate Welch's PSD.

The median oscillation frequency of the eyes was plotted against the median oscillation frequency of the RGCs and fitted with a linear regression model.

Spike train synchrony. Synchronization between spike trains was quantified using SPIKE-Synchronization. This time scale-independent and parameter-free metric uses Inter-Spike-Interval derived coincidence windows to generate a similarity score. A similarity score of 1 occurs only if each spike in a train has a matching spike in the other train(s) whereas a score of 0 occurs only if the spike trains do not contain any coincidences (for more details see: Kreuz et al., 2015; Satuvuori et al., 2017). The analysis routine was used within cSPIKE, a publicly available Matlab-based spike train analysis software package (https://thomas-kreuz.complexworld.net/source-codes/cspike).

We generated two distributions of similarity scores for each retina. The first distribution was of similarity scores between spike trains of spontaneous activity occurring in the dark for units within the same retina. The spontaneous activity was divided into 5 s long non-overlapping periods and for each of these periods the similarity scores for each unit *vs*. every other unit wee determined (e.g. a 15 min recording of 30 units resulted in $30 \times 30 \times 180$ similarity scores). For these same units we also generated a second distribution of similarity scores, this time comparing their spike trains with those of units from different retinas in the other treatment groups. For example, units from a single *Ca*$_v$*1.4-KO* retina were compared with unrelated units from all the *Nyx*^{nob}, WT and *Grm6*^{nob3} retinas, again using 5 s long non-overlapping periods. This second population of similarity scores was used to estimate the chance distribution of similarity scores occurring for units whose activity is unrelated.

For each retina, we quantified the distance between their two distributions of similarity scores using the Hellinger distance. The relative probability distribution of the similarity scores was distributed over 51 equally spaced bins ranging from 0 to 1 in 0.02 increments, and for the two discrete probability distributions $P = (p_1,\ldots p_k)$ and $Q = (q_1,\ldots q_k)$, their Hellinger distance was then defined as

$$H(P, Q) = \frac{1}{\sqrt{2}}\sqrt{\sum_{i=1}^{k}\left(\sqrt{p_i} - \sqrt{q_i}\right)^2}$$

where 1 indicates there is no overlap of the populations and 0 indicates the two populations fully overlap.

Statistical analysis

Statistical analysis was performed using SPSS Statistics 28 (IBM Corp., Armonk, NY, USA) and Origin Pro 8 (Northampton, MA, USA). Since the distribution of the frequencies of eye movement oscillations violated the assumption of normality (Shapiro Wilk), statistical differences were assessed using an independent-samples Mann–Whitney *U* test. All values are given as median ± MAD (median absolute deviation) and a statistically significant difference was assumed at $P < 0.05$. Statistical differences in the Hellinger distances were tested by a one-way ANOVA with a *post hoc* Bonferroni test. To test whether there is a statistically significant effect of light intensity on oscillation frequency we used a Wilcoxon signed-rank test.

Computational model

The schematic shown in Fig. 7*Aa* below gives an overview of the BC, A_{II} AC and RGC network we simulated. An A_{II} AC is electrically coupled to an ON-CBC and to other A_{II} ACs via gap junctions (Marc et al., 2014). A_{II} ACs receive glutamatergic input from ON-RBCs (Marc et al., 2014) and are inhibited by the OFF-CBC-driven OFF-ACs (Marc et al., 2014). This latter pathway is a so-called crossover inhibition pathway. Light stimulation leads to depolarization of the ON-BCs and thus to depolarization of the A_{II} ACs. In addition, the OFF-CBCs and subsequently the OFF ACs hyperpolarize upon light

stimulation and this will lead to a decrease of the inhibition of the A_{II} ACs, further depolarizing the A_{II} ACs. ON-CBCs generate an output to ON RGCs and OFF-BCs generate an output to OFF RGCs. All of the described cell types are distributed in a hexagonal grid.

To reduce the number of free parameters and computation time, we simplified the model (see Fig. 7*Ab*). The ON-RBCs are simulated by steady current injections since we simulate photopic conditions. The inhibitory input from the OFF pathway is implemented as a steady current injection into the A_{II} Acs. Similarly, the photoreceptor input to the ON-CBCs was simulated as a steady current injection into the ON-CBCs. The output of the ON-CBCs is the input to ON-RGCs and the OFF-RGCs are the inverse of ON-RGCs.

Each ON-CBC contacts one A_{II} AC, and each A_{II} AC in turn contacts one RGC and six A_{II} ACs. The literature shows that one A_{II} AC is contacted by 10 ON-CBCs (Sigulinsky et al., 2020). This physiological connectivity was implemented by scaling the coupling conductances. Next, we present the equations describing the various cell types (see Fig. 7*Ab*).

A_{II} AC model. The A_{II} AC was simulated as a three-compartment model (Choi et al., 2014) consisting of a soma, an initiation site and a connecting cable (see Fig. 7*Aa*). The arboreal dendrites are part of the soma. The ionic currents are described by Hodgkin–Huxley type equations.

The sodium current (I_{Na}) is given by

$$I_{Na} = G_{Na}\, m_{Na}^3 h_{Na}\, (V - E_{Na})$$

where the gating variables are

$$\tau_{mNa}\, \frac{dm_{Na}}{dt} = m_{\infty Na}\, - m_{Na}$$

$$\tau_{hNa}\, \frac{dm_{Na}}{dt} = h_{\infty Na}\, - h_{Na}$$

with

$$m_{\infty Na}\ (V) = \left(1 + e^{-\frac{V+48}{5}}\right)^{-1}$$

$$h_{\infty Na}\ (V) = \left(1 + e^{-\frac{V+49.5}{2}}\right)^{-1}$$

The M-type potassium current (I_M) is given by

$$I_M = G_M\, m_M\, (V - E_K)$$

where the gating variables are

$$\tau_{mM}\, \frac{dm_M}{dt} = m_{\infty M}\, - m_M$$

with

$$m_{\infty M}\ (V) = \left(1 + e^{-\frac{V+40}{4}}\right)^{-1}$$

The A-type potassium current (I_A) is given by

$$I_A = G_A\, m_A\, (ch_{1A} + (1 - c)\, h_{2A})\, (V - E_K)$$

$$c\ =\ \left(1 + e^{-\frac{V+45}{15}}\right)^{-1}$$

where the gating variables are

$$\tau_{mA}\, \frac{dm_A}{dt} = m_{\infty A}\, - m_A$$

$$\tau_{h_{1A}}\, \frac{dh_{1A}}{dt} = h_{\infty A}\, - h_{1A}$$

$$\tau_{h_{2A}}\, \frac{dh_{2A}}{dt} = h_{\infty A}\, - h_{2A}$$

with

$$m_{\infty A}\ (V) = \left(1 + e^{-\frac{V+10}{7}}\right)^{-1}$$

$$h_{\infty A}\ (V) = \left(1 + e^{-\frac{V+40.5}{2}}\right)^{-1}\ + \left(1 - f\right)$$

$$\tau_{h_{1A}}\ (V) =\ 25 - 20\left(1 + e^{-\frac{V+35}{6}}\right)^{-1}$$

$$\tau_{h_{2A}}\ (V) =\ min\left[\frac{(V+17)^2}{4} + 26,\ 100\right]$$

Next to these ionic currents there is a leak current

$$I_{leak,AII} =\ \bar{g}_{leak}\, (V - E_{leak})$$

The ON-CBCs are coupled to A_{II} ACs by gap junctions. For computational reasons, we simulated only one ON-CBC per A_{II} AC. To account for the fact that 10 ON-CBCs are coupled to one A_{II} AC, we made the coupling conductance seen by the A_{II} ACs 10 times larger than the conductance seen by the ON-CBC.

A_{II} ACs are coupled by gap junctions to each other in a hexagonal network such that each A_{II} AC is coupled to six other A_{II} ACs. The gap junction currents are given by

$$I_{GJ} =\ G_{GJ}\left(V_{Coupled} - V\right)$$

and summed in a total gap junction current per cell $I_{GJ\text{-total}}$.

The membrane potentials of the three compartments were calculated as

$$C\, \frac{dV_{IS}}{dt} =\ -\left(I_{Na} + I_A + I_M + I_{leak}\right) + I_{compart}$$

$$C\, \frac{dV_{Soma}}{dt} =\ -\left(I_A + I_{leak}\right) + I_{compart} + I_{GJ} + I_{inject}$$

$$C\, \frac{dV_{cable}}{dt} =\ -I_{leak} + I_{compart}$$

ON-CBC model. For the ON-CBC, we used the model from Usui et al. (1996). This model consists of a delayed rectifying potassium current (I_{Kv}), a transient potassium current (I_A), a hyperpolarization activated current (I_h), a calcium current (I_{Ca}) and a calcium-dependent potassium current (I_{KCa}). A two-compartment model was used for the internal calcium concentration of the ON-CBC, which is needed to calculate I_{KCa}. One compartment was close to the membrane and consisted of a fast and a slow calcium buffer, and two exchange currents. The other compartment was within the cell and consisted of only the two calcium buffers. Calcium will flow from one compartment into the other by diffusion.

All ionic currents are described with Hodgkin–Huxley-type equations, except for I_h which is described with a Markov chain-type model.

The delayed rectifying potassium current (I_{Kv}) current is described by

$$I_{Kv} = G_{Kv} {m_{Kv}}^3 h_{Kv} (V - E_k)$$

where the gating variables are calculated as

$$\frac{dm_{Kv}}{dt} = \alpha_{mKv} (1 - m_{Kv}) - \beta_{mKv} m_{Kv}$$

$$\frac{dh_{Kv}}{dt} = \alpha_{hKv} (1 - h_{Kv}) - \beta_{hKv} h_{Kv}$$

with

$$\alpha_{mKv} = \frac{400}{1 + e^{-\frac{V-15}{36}}}$$

$$\beta_{mKv} = e^{-\frac{V}{13}}$$

$$\alpha_{hKv} = 0.3 \cdot 10^{-3} \cdot e^{-\frac{V}{7}}$$

$$\beta_{hKv} = \frac{80}{1 + e^{-\frac{V+115}{15}}} + 0.02$$

The transient potassium current (I_A) is modelled with Hodgkin–Huxley type equations, and is defined as

$$I_A = G_A m_A^3 h_A (V - E_K)$$

with the gating variables

$$\frac{dm_A}{dt} = \alpha_{mA} (1 - m_A) - \beta_{mA} m_A$$

$$\frac{dh_A}{dt} = \alpha_{hA} (1 - h_A) - \beta_{hA} h_A$$

where

$$\alpha_{mA} = \frac{1200}{1 + e^{-\frac{V-50}{28}}}$$

$$\beta_{mA} = 6\, e^{-\frac{V}{10}}$$

$$\alpha_{hA} = 45 \cdot 10^{-3} e^{-\frac{V}{13}}$$

$$\beta_{hA} = \frac{75}{1 + e^{-\frac{V+50}{15}}}$$

The hyperpolarization activated current (I_h) is described with a Marko chain-like model which described the transition between open and closed states. The current is given by

$$I_h = G_h\, m_h\, (V - E_h)$$

where the total open probability is the sum of the open states

$$m_h = O_1 + O_2 + O_3$$

The open and closed states are calculated as

$$\frac{dM}{dt} = KM$$

where

$$M = \begin{pmatrix} C_1 \\ C_2 \\ O_1 \\ O_2 \\ O_3 \end{pmatrix}$$

$$K = \begin{bmatrix} -4\alpha_h & \beta_h & 0 & 0 & 0 \\ 4\alpha_h & -(3\alpha_h + \beta_h) & 2\beta_h & 0 & 0 \\ 0 & 3\alpha_h & -(2\alpha_h + 2\beta_h) & 3\beta_h & 0 \\ 0 & 0 & 2\alpha_h & -(\alpha_h + 3\beta_h) & 4\beta_h \\ 0 & 0 & 0 & \alpha_h & -4\beta_h \end{bmatrix}$$

with the transition rate constants defined as

$$\alpha_h = \frac{3}{1 + e^{\frac{V+110}{15}}}$$

$$\beta_h = \frac{1.5}{1 + e^{-\frac{V+115}{15}}}$$

The calcium current (I_{Ca}) is given by

$$I_{Ca} = G_{Ca} m_{Ca}^4 h_{Ca} (V - E_{Ca})$$

with a reversal potential dependent on the calcium concentration

$$E_{Ca} = 12.9 \log \left(\frac{[Ca^{2+}]_o}{[Ca^{2+}]_s} \right)$$

with the gating variables

$$\frac{dm_{Ca}}{dt} = \alpha_{mCa} (1 - m_{Ca}) - \beta_{mCa} m_{Ca}$$

$$\frac{dm_{Ca}}{dt} = \alpha_{mCa} (1 - m_{Ca}) - \beta_{mCa} m_{Ca}$$

where

$$\alpha_{mCa} = \frac{1200(120 - V)}{e^{\frac{120-V}{25}} - 1}$$

$$\beta_{mCa} = \frac{40 \cdot 10^3}{1 + e^{\frac{V+68}{25}}}$$

$$h_{Ca} = \frac{e^{-\frac{V-50}{11}}}{1 + e^{-\frac{V-50}{11}}}$$

The calcium-dependent potassium current (I_{KCa}) is given by

$$I_{KCa} = \bar{g}_{Kc}\, m_{Kc}^2 m_{Kc1}\, (V - E_K)$$

where the gating variables are described as

$$\frac{dm_{Kc}}{dt} = \alpha_{mKc}\ (1 - m_{Kc}) - \beta_{mKc} m_{Kc}$$

$$m_{Kc1} = \frac{\left[Ca^{2+}\right]_s}{[Ca^{2+}]_s + 0.2}$$

with

$$\alpha_{mKc} = \frac{100 \cdot (230 - V)}{e^{\frac{(230-V)}{52}} - 1}$$

$$\beta_{mKc} = e^{-\frac{V}{95}}$$

$$m_{Kc1} = \frac{\left[Ca^{2+}\right]_s}{[Ca^{2+}]_s + 0.2}$$

The change in calcium concentration close to the membrane ($[Ca^{2+}]_s$) is described as

$$\begin{aligned}\frac{d\left[Ca^{2+}\right]_s}{dt} = & -\frac{I_{Ca}}{2F\ V_s} - \frac{D_{Ca}\ S_{sd}}{V_s\ d_{sd}}\left(\left[Ca^{2+}\right]_s - \left[Ca^{2+}\right]_d\right) \\ & - \frac{(I_{ex} - I_{ex2})}{2F\ V_s} + \beta_{bl}\left[Ca^{2+}\right]_{bls} - \alpha_{bl}\left[Ca^{2+}\right]_s \\ & \left(\left[Ca^{2+}\right]_{blmax} - \left[Ca^{2+}\right]_{bls}\right) + \beta_{bh}\left[Ca^{2+}\right]_{bhs} \\ & -\alpha_{bh}\left[Ca^{2+}\right]_s\ \left(\left[Ca^{2+}\right]_{bhmax} - \left[Ca^{2+}\right]_{bhs}\right)\end{aligned}$$

and the calcium concentration inside the cell ($[Ca^{2+}]_d$) as

$$\begin{aligned}\frac{d\left[Ca^{2+}\right]_d}{dt} = & \frac{D_{Ca}\ S_{sd}}{V_d\ d_{sd}}\ \left(\left[Ca^{2+}\right]_s - \left[Ca^{2+}\right]_d\right) + \beta_{bl}\left[Ca^{2+}\right]_{bld} \\ & -\alpha_{bl}\left[Ca^{2+}\right]_d\ \left(\left[Ca^{2+}\right]_{blmax} - \left[Ca^{2+}\right]_{bld}\right) \\ & + \beta_{bh}\left[Ca^{2+}\right]_{bhd} - \alpha_{bh}\left[Ca^{2+}\right]_d\ \left(\left[Ca^{2+}\right]_{bhmax} \right. \\ & \left. - \left[Ca^{2+}\right]_{bhd}\right)\end{aligned}$$

where

$$\frac{d[Ca^{2+}]_{bls}}{dt} = \alpha_{bl}[Ca^{2+}]_s\ ([Ca^{2+}]_{blmax} - [Ca^{2+}]_{bls}) - \beta_{bl}[Ca^{2+}]_{bls}$$

$$\begin{aligned}\frac{d\left[Ca^{2+}\right]_{bhs}}{dt} = & \alpha_{bh}\left[Ca^{2+}\right]_s\ \left(\left[Ca^{2+}\right]_{bhmax} \right. \\ & \left. - \left[Ca^{2+}\right]_{bhs}\right) - \beta_{bh}\left[Ca^{2+}\right]_{bhs}\end{aligned}$$

$$\begin{aligned}\frac{d\left[Ca^{2+}\right]_{bld}}{dt} = & \alpha_{bl}\left[Ca^{2+}\right]_d\ \left(\left[Ca^{2+}\right]_{blmax} \right. \\ & \left. - \left[Ca^{2+}\right]_{bld}\right) - \beta_{bl}\left[Ca^{2+}\right]_{bld}\end{aligned}$$

$$\begin{aligned}\frac{d\left[Ca^{2+}\right]_{bhd}}{dt} = & \alpha_{bh}\left[Ca^{2+}\right]_d\ \left(\left[Ca^{2+}\right]_{bhmax} \right. \\ & \left. - \left[Ca^{2+}\right]_{bhd}\right) - \beta_{bh}\left[Ca^{2+}\right]_{bhd}\end{aligned}$$

with the exchange currents defined as

$$I_{ex} = \frac{J_{ex}\ \left(\left[Ca^{2+}\right]_s - \left[Ca^{2+}\right]_{min}\right)}{[Ca^{2+}]_s - [Ca^{2+}]_{min} + 2.3}\ \exp\left(-\frac{V + 14}{70}\right)$$

$$I_{ex2} = \frac{J_{ex2}\ \left(\left[Ca^{2+}\right]_s - \left[Ca^{2+}\right]_{min}\right)}{[Ca^{2+}]_s - [Ca^{2+}]_{min} + 0.5}$$

Finally, we added a leak current

$$I_l = G_l\ (V - E_l)$$

The gap junction between the ON-CBC and the A_{II} AC is given by

$$I_{GJ} = G_{GJ}\left(V_{Coupled} - V\right)$$

We only simulate one ON-CB per A_{II} cell. The membrane potential of the BC is given by

$$\begin{aligned}C\ \frac{dV_{BC}}{dt} = & -(I_{Kv} + I_A + I_h + I_{Ca} + I_{KCa} + I_{leak}) \\ & + I_{GJ} + I_{inject}\end{aligned}$$

RGC model. The RGC model is a simple spike-generating mechanism consisting of three ion channels, a sodium current, an M-type potassium current, an A-type potassium channel and a leak current. Additionally to these ion channels there is a synaptic current which is modelled as a current that is dependent on the calcium current of the bipolar cell. The sodium channel, M-type potassium channel and A-type potassium channels are described with the same equation used for the A_{II} ACs. The synaptic current is given by

$$I_{synapse} = G_{synapse} \cdot I_{Ca\ ONCB} \cdot (V + 35)$$

The membrane potential of the RGC is given by

$$C\ \frac{dV_{RGC}}{dt} = -\left(I_{Na} + I_M + I_A + I_{leak} + I_{synapse}\right)$$

For the OFF RGC, the voltage dependency of $I_{synapse}$ is inverted and the leak current is adjusted in order to depolarize the RGC membrane potential:

$$I_{synapse} = G_{synapse} \cdot I_{Ca\ ONCB} \cdot -V$$

Model parameters for the ion channels and the various capacitances are given in Table 1. The parameters for the

Table 1. Parameters for the ion channels and membrane capacitances of the various cell types; these parameters are the same for each animal model

Parameter	Value	Parameter	Value
A_{II}		ON-CBC	
Sodium current		C	10 pF
E_{Na}	50 mV	*Delayed rectifying potassium current*	
τ_{mNa}	0.01 ms	G_{Kv}	2 nS
τ_{hNa}	0.5 ms	E_{Kv}	−58 mV
M-type potassium current		*The transient potassium current*	
E_k	−77	G_A	35 nS
τ_{mM}	50 ms	E_K	−58 mV
A-type potassium current		*Hyperpolarization activated current*	
E_k	−77 mV	G_h	5.975 nS
τ_{mA}	1 ms	E_h	−17.7 mV
		Calcium current	
Soma		G_{Ca}	1.1
C	1.96×10^{-8} F	$[Ca^{2+}]_o$	2000 μM
G_A	7.9×10^{-8} S	*Calcium dependent potassium current*	
G_{leak}	4.9×10^{-10} S	G_{Kc}	8.5 nS
E_{leak}	−65 mV	E_K	−58 mV
$G_{GJ\text{-}A2\text{-}BC}$	200×10^{-9} S	*Leak current*	
$G_{compart}$	2.9×10^{-9} S	G_l	0.5 nS
		E_l	−50 mV
Initiation site		*Gap-junction*	
C	1.26×10^{-12} F	$G_{GJ\text{-}A2\text{-}BC}$	20 nS
G_{Na}	2.5×10^{-8} S		
G_A	1×10^{-8} S	ON-RGC	
G_M	3.77×10^{-9} S	C	1.26×10^{-10} S
G_{leak}	3.14×10^{-12} S	E_k	−77 mV
E_{leak}	−65 mV	E_{Na}	50 mV
$G_{compart}$	2.9×10^{-9} S	E_{leak}	−100 mV
		g_{leak}	3.1×10^{-12} S
Cable		G_{syn}	10×10^{-12} S
G_{leak}	7.54×10^{-12} S		
E_{leak}	−65 mV	OFF-RGC	
$G_{compart}$	2.9×10^{-9} S	E_{leak}	300 mV
		G_{leak}	3.1×10^{-12} S
		G_{syn}	75×10^{-12} S

calcium buffers are presented in Table 2. Table 3 gives the current injections for the different mouse models, the bias current and the light step current.

Results

Oscillating eye movements in *Grm6^{nob3}* and *Ca$_v$1.4-KO* mice compared to those in *Nyx^{nob}* mice

To investigate whether there is a common cause for nystagmus in CSNB we first measured the eye movements of WT, *Grm6^{nob3}*, *Nyx^{nob}* and *Ca$_v$1.4-KO* mice. Figure 2 shows example raw traces of the horizontal eye position for each of these mice in response to a monocularly presented horizontal moving vertical grating. WT mice show a normal OKR. They successfully follow the grating in the temporal to nasal direction (6–10 s), keep their eyes still when the stimulus is stationary (4–6 s) and do not follow the grating when it moves in the nasal to temporal direction (0–4 s).

On the other hand, the OKRs of *Grm6^{nob3}*, *Nyx^{nob}* and *Ca$_v$1.4-KO* mice were severely impaired and had different characteristics in each mutant. *Grm6^{nob3}* and *Nyx^{nob}* mice initially follow the gratings moving in the temporal to nasal direction (arrows in Fig. 2), but were unable to maintain this eye movement (also see Winkelman et al., 2019). Furthermore, their eyes tended to drift when the grating stopped moving. The *Ca$_v$1.4-KO* mice lacked an OKR altogether but did exhibit a random slow drift in eye position. However, all mutants showed the presence of small-amplitude high-frequency eye movement

Table 2. Parameters of the Ca^{2+} buffer system; these parameters are the same for each animal model

Parameter	Value
Calcium buffer	
F	9.649×10^4
V_s (volume)	1.692×10^{-14} dm^3
V_d	7.356×10^{-14} dm^3
D_{Ca}	6×10^{-8} dm^2/s
α_{bl}	0.4 (s·μM)$^{-1}$
α_{bh}	100 (s·μM)$^{-1}$
β_{bl}	0.2 (s·μM)$^{-1}$
β_{bh}	90 (s·μM)$^{-1}$
J_{ex}	9 pA
J_{ex2}	9.5 pA
Ca_{min}	0.05 μM
S_{sd}	4×10^{-8} dm^2
d_{sd}	5.9×10^{-5} dm^2

oscillations, i.e. pendular nystagmus. In this study we will focus only on these small-amplitude eye movement oscillations and not discuss the OKR further.

Using PSD plots, we quantified the nystagmus under four stimulus conditions: darkness, homogeneous illumination, vertical gratings moving horizontally and horizontal gratings moving horizontally (Fig. 3). While the eyes of *Grm6^{nob3}* and *Nyx^{nob}* mice only oscillate when stimulated with a vertical grating, *Ca$_v$1.4-KO* mice show oscillatory eye movements under all stimulus conditions (arrows). Furthermore, the frequency of the eye movement oscillations during the vertical grating condition differs between the three genotypes [median ± MAD; *Grm6^{nob3}*: 3.4 ± 0.38 Hz (N = 12); *Nyx^{nob}*: 5.0 ± 0.25 Hz (N = 7); *Ca$_v$1.4*-KO; 8.0 ± 0.38 Hz (N = 6); Mann–Whitney U test, $P_{Grm6nob3,Nyxnob} = 0.001$; $P_{Grm6nob3,Cav1.4\text{-}KO} = 1.8 \times 10^{-4}$; $P_{Nyxnob,Cav1.4\text{-}KO} = 0.001$). Additionally, the power spectra of all knockout mice also show a low-frequency peak representing a slow eye movement drift, which will not be discussed further. WT mice on the other hand do not exhibit comparable eye movement oscillations although a very small peak at around 5 Hz may be observed sometimes in their power spectrum.

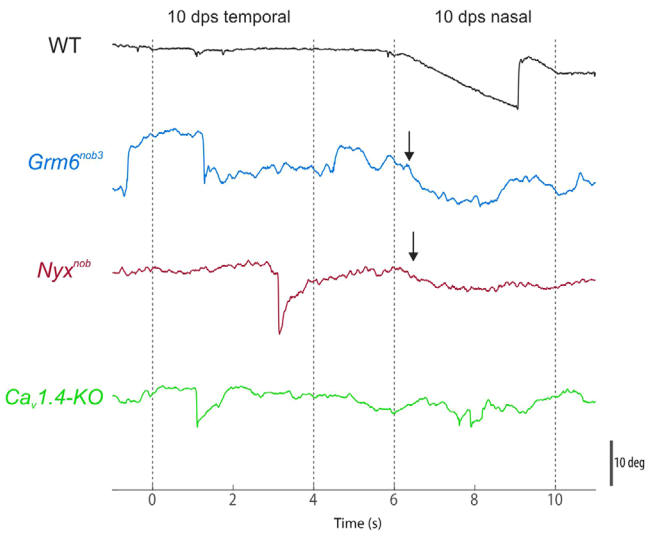

Figure 2. Example horizontal eye movement traces for a WT, *Grm6^{nob3}*, *Nyx^{nob}* and *Ca$_v$1.4-KO* mouse in response to a vertical sinusoidal grating presented to the left eye
All three mouse models show small oscillatory eye movements.

Taken together, the eye movement data shown in Fig. 3 reveal phenotypical differences between the various CSNB mutants. How does this correlate with RGC activity?

Spontaneous oscillation frequencies of *Grm6^{nob3}*, *Ca$_v$1.4-KO* and *Nyx^{nob}* mice differ

Previously, we have shown that the RGCs of *Nyx^{nob}* mice fire in an oscillatory fashion with a frequency closely matching that of their pendular nystagmus. The causality of this relationship was shown using retina-specific pharmacological treatments that changed the oscillation frequency of RGC firing resulting in a similar change in frequency of the nystagmus (Winkelman et al., 2019). To test whether a similar relationship between RGC oscillations and nystagmus exists in the various mutants, we determined their RGC oscillatory firing frequency.

In the dark, the spontaneous activity (Fig. 4*A*) of 59.1 ± 29.16% (mean ± SD, N = 8 mice) *Nyx^{nob}* and *47.2* ± 14.17% *Ca$_v$1.4-KO* (N = 4 mice) RGCs was oscillatory as indicated by the periodic variations in their autocorrelations (Fig. 4*B*) and peaks in their PSD plots (Fig. 4*C*). For *Nyx^{nob}* mice, their RGCs oscillated at a lower frequency (median ± MAD; 7.8 ± 0.25 Hz, n = 368 RGCs, N = 8 mice) compared to those of the *Ca$_v$1.4-KO* mice (median ± MAD; 11.8 ± 1.25 Hz, n = 135 RGCs, N = 4 mice, Mann–Whitney U test, $P_{Nyxnob,\ Cav1.4\text{-}KO} = 0.000$). Unexpectedly, the autocorrelations and PSD of *Grm6^{nob3}* RGCs showed no evidence of oscillatory activity and were instead comparable to that of WT animals.

Light-induced oscillations in *Grm6^{nob3}* RGCs

As we showed previously, in *Nyx^{nob}* mice, individual RGCs oscillate at similar frequencies, but their activity is asynchronous in the dark. Light stimulation phase resets the RGC oscillations, and then this synchronized oscillatory retinal output induces oscillating eye movements (Winkelman et al., 2019). For *Grm6^{nob3}* mice, could light stimulation still induce synchronized RGC oscillations even though their activity is not spontaneously

Table 3. Bias currents for the A_{II} ACs; injected currents for each animal model; currents to simulate the light steps

	Genotype	Value
Current injected into ON-CBC for the different animal models	*Grm6^{nob3}*	100×10^{-12} A
	Nyx^{nob}	500×10^{-12} A
	Ca$_v$1.4-KO	700×10^{-12} A
Bias current A_{II} ACs		300×10^{-12} A multiplied with a random number between −1 and 1
Light step current		1500×10^{-12} A

oscillatory in the dark? To answer this question, we studied the responses of RGCs to a light flash (Fig. 5).

As expected, a light flash stimulus induced typical ON and OFF light responses in WT mice without RGC oscillations (Fig. 5*A*–*C*). This was not the case for *Grm6^{nob3}* and *Nyx^{nob}* mice, which lack the RGC ON light response but showed oscillatory activity briefly after the light stimulation onset. In the *Grm6^{nob3}* mouse only 6.2 ± 4.95% (mean ± SD, $N = 3$ mice) of the RGCs oscillated, in *Nyx^{nob}* 36.5 ± 13.95% ($N = 7$ mice) and in *Ca$_v$1.4-KO* 22.2 ± 12.89% ($N = 4$ mice) oscillated. As is also the case for *Nyx^{nob}* mice, RGCs in the *Grm6^{nob3}* mice showed oscillations directly after stimulus onset. Two groups of RGCs were found that oscillated in counter-phase presumably originating from ON- and OFF-RGCs (Fig. 4,5*B* and *C*).

For *Grm6^{nob3}* mice, the duration of the light flash-induced RGC oscillations was much shorter than it was in *Nyx^{nob}* mice (Fig. 5*B* and *C*). Furthermore, *Nyx^{nob}* RGCs oscillated at a higher frequency than *Grm6^{nob3}* RGCs (median ± MAD, *Nyx^{nob}*: 8 ± 1.0 Hz, $n = 245$, $N = 7$; *Grm6^{nob3}*: 6 ± 1.0 Hz, $n = 17$, $N = 3$, Mann–Whitney U test, $P_{\text{Nyxnob, Grm6nob3}} = 4.3 \times 10^{-8}$). Hence, light stimulation can induce synchronized RGC oscillations in *Grm6^{nob3}* mice, but they are phenotypically distinct from those of *Nyx^{nob}* mice.

RGCs and eye movements oscillated at similar frequencies

Next, we determined how well the oscillation frequency of RGC activity matched that of the eye movements for the *Grm6^{nob}*, *Nyx^{nob}* and *Ca$_v$1.4-KO* animals. For this we used the oscillation frequency of RGC activity during the light flash, and of eye movements during the vertical grating, as these were the only conditions in which oscillatory responses occurred in each of the three models. Fig. 5*E* shows the relationship between the eye movement oscillation frequency and the RGC oscillation frequency. In general, the RGC oscillation frequency was linearly related to the eye movement oscillation frequency, but the RGC oscillation frequency was slightly higher than that of the eye movements.

RGC oscillations in the *Ca$_v$1.4-KO* are synchronized under all stimulus conditions

Ca$_v$1.4-KO mice exhibited nystagmus in the four stimulus conditions (Fig. 3), whereas *Grm6^{nob3}* and *Nyx^{nob}* mice showed this behaviour only for the vertical grating. This suggests the *Ca$_v$1.4-KO* oscillatory eye movements occur independently from a visual stimulus. The *Ca$_v$1.4-KO* mice also lacked an OKR response (Fig. 2) and their RGCs did not respond to a light flash stimulus (Fig. 5*A*–*C*), which suggests that these mice are blind. How then can the RGCs oscillations in *Ca$_v$1.4-KO* mice be synchronized? A possibility is that unlike *Grm6^{nob3}* and *Nyx^{nob}* mice, the RGCs in *Ca$_v$1.4-KO* mice display a degree of inherent synchronization independent of the stimulus condition.

To test this, we assessed to what extent the spontaneous activity of RGCs was synchronized in the dark for each of the mouse models. Using the SPIKE-synchronization metric (https://thomas-kreuz.complexworld.net/source-codes/cspike), we determined two synchronization score distributions for each retina (Fig. 4*D*). The first set of scores measured the synchronization occurring between activity of RGCs from the same retina. The second set was generated by comparing the activity of these same RGCs with that of RGCs from the three other mouse models, giving an estimate of the chance distribution of synchronization scores for the retina. We then quantified the difference between these two distributions using the Hellinger distance (Fig. 4*E*).

Ca$_v$1.4-KO retinas had distributions that shifted towards higher synchronization scores for RGCs in the same retina *versus* unrelated retinas, compared to the three other mouse models (Fig. 4*D*). Indeed, the lowest Hellinger distance for the *Ca$_v$1.4-KO* retinas was greater than the highest Hellinger distance of any other group (Fig. 4*E*, one-way ANOVA, $P_{\text{WT, Cav1.4-KO}} = 0.0003$, $P_{\text{Grm6nob3, Cav1.4-KO}} = 0.0001$, $P_{\text{Nyxnob, Cav1.4-KO}} = 0.0003$, $P_{\text{WT,Nyxnob}} = 1$, $P_{\text{WT, Grm6nob3}} = 1$, $P_{\text{Grm6nob3, Nyxnob}} = 1$). Furthermore, only the *Ca$_v$1.4-KO* group demonstrated elevated synchronization scores within the same retina. These outcomes indicate that there is a degree of inherent synchronization in the spontaneous activity of *Ca$_v$1.4-KO* RGCs that is not present in *Grm6^{nob3}*, *Nyx^{nob}* or WT conditions.

A_{II} ACs as a potential cause for the difference in eye movement oscillations

Previously, we have shown evidence suggesting A_{II} ACs are driving the oscillatory responses of RGCs (Winkelman et al., 2019). A_{II} ACs oscillate when they are outside their normal membrane potential range and the oscillation frequency increases with depolarization (Choi et al., 2014). If this is the case then depolarizing Nyx^{nob} A_{II} ACs further should lead to an increase of the oscillation frequency of their RGCs. To test this hypothesis, we recorded the light-induced oscillations of Nyx^{nob} RGCs at two different light intensities (Fig. 6). Consistent with our expectations, we found that when A_{II} ACs are depolarized more strongly by a light flash of higher light intensity, the RGC oscillation frequency increases by about 1.1 ± 0.91 Hz (median ± MAD, n = 92 RGCs, $N = 4$ mice). This increase in oscillation frequency was statistically significant (Wilcoxon signed-rank test: $Z = -4.179$, $P = 2.9 \times 10^{-5}$, $n = 92$ RGCs, $N = 4$ mice).

Computational model

To determine whether the various phenotypes could be generated by only changes in ON-BC input to the A_{II} AC, we constructed a computational model consisting of a grid of hexagonally arranged units consisting of an ON-CBC

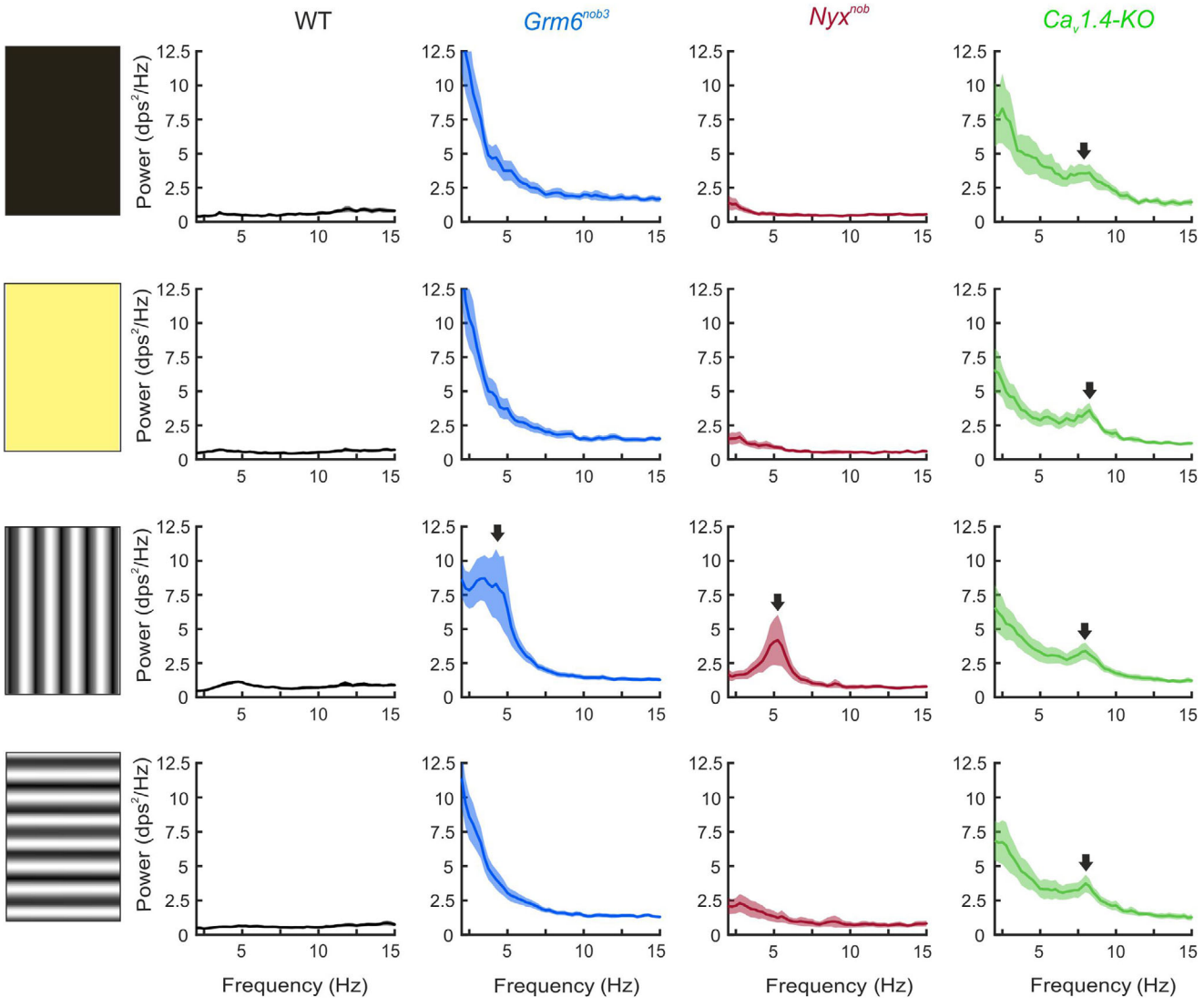

Figure 3. Power spectra comparing the horizontal eye movements of WT (*N* = 7), *Grm6*^{nob3} (*N* = 12), *Nyx*^{nob} (*N* = 7) and *Ca*$_v$*1.4-KO* (*N* = 7) mice in darkness, under homogenous light as well as with vertical and horizontal bar stimulations
Only stimulation with a vertical grating induces oscillatory eye movements in *Grm6*^{nob3} and *Nyx*^{nob} mice while the eyes of *Ca*$_v$*1.4-KO* mice are oscillating under all stimulus conditions.

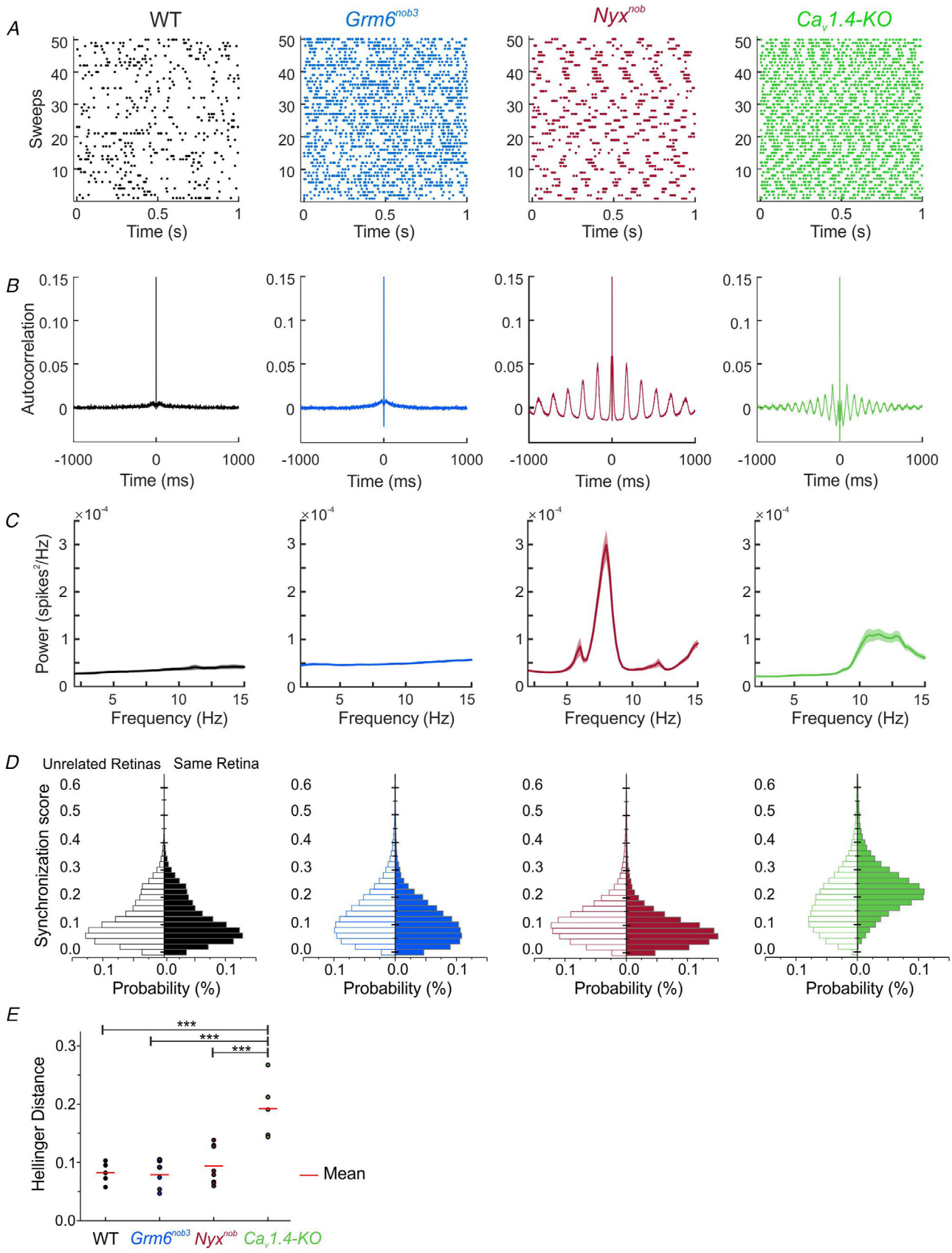

Figure 4. Comparison of the spontaneous RGC activity of WT, *Grm6^{nob3}*, *Nyx^{nob}* and *Ca$_V$1.4-KO* mice

A, raster plots comparing the extracellularly recorded spontaneous spiking activity for, in each case, one RGC from WT, *Grm6*^{nob3}, *Nyx*^{nob} (red) and *Ca*$_v$*1.4*-KO. *B*, autocorrelation of activity of the same RGC as in *A* showing oscillatory behaviour visible as periodic variations, only for the *Nyx*^{nob} and *Ca*$_v$*1.4-KO* mice but not WT or *Grm6*^{nob3} RGCs. *C*, mean power spectra of the spontaneous activity in WT (n = 209 RGCs from N = 5 mice), *Grm6*^{nob3} (n = 543 RGCs from N = 11 mice), *Nyx*^{nob} (n = 367 RGCs from N = 8 mice) and *Ca*$_v$*1.4-KO* (n = 135 RGCs from N = 4 mice). *D*, comparison of similarity scores as a measure for synchrony for spike trains from RGCs from the same *versus* from another retina. In the *Ca*$_v$*1.4-KO* retina RGCs are synchronized in the dark which is not the case for the other three mice. *E*, comparison of the Hellinger distance of WT and the three mouse models. ***$P < 0.001$.

coupled electrically to an A_{II} AC and synaptically to an ON- RGC. A detailed model description is presented in the Material and methods.

Figure 7*Aa* shows how the various relevant cell types are connected in the retina. The ON- and OFF-CBCs receive synaptic input from the cone photoreceptors, while the ON-RBC receives its input from the rod photoreceptor. The ON-CBCs are electrically coupled via gap junctions to the A_{II} AC while the ON-RBCs give synaptic glutamatergic input to the A_{II} ACs. The OFF-CBC projects directly to the OFF-RGC and via an inhibitory AC to the A_{II} AC. We simulated a simplified version of this network (see Material and methods; Fig. 7*Ab*).

Fig. 7*Ba–e* gives an overview of the model response to a light flash. The heart of the model is the A_{II} AC. When depolarized beyond their normal working range they start to oscillate. Previously, we showed that individual RCGs oscillate at slightly different frequencies (Winkelman et al., 2019). To simulate this we injected each of the A_{II} ACs with a small sustained current, but varied the magnitude of each of the sustained currents randomly. This resulted in all A_{II} ACs oscillating at slightly different frequencies. Fig. 7*Ba* shows example traces of six A_{II} ACs, all slightly displaced along the *y*-axis for clarity. The A_{II} ACs oscillations are transmitted via gap junctions to the ON-CBS. Fig. 7*Bb* shows the response to a light flash of a single ON-CBC (blue line) and a connected ON-RGC (red line). ON-CBCs show small oscillations and as a result the ON-RGC generates a burst of spikes on the upward flank of the CBC oscillations. Fig. 7*Bc* shows six CBCs, all oscillating with slightly different frequencies. A raster plot of the spikes and the sum of the spikes generated in an ON-RGC are shows in Fig. 7*Bd* and *e*.

In the dark, RGCs are oscillating but the oscillations are not synchronized. A simulated light flash with a duration of 4 s presented at $t = 4$ s causes most RGC oscillations to phase reset and synchronize for a brief period. This mimics the behaviour of the RGC recordings. Finally, the PSD plots in Fig. 7*C* show that RGCs oscillate at higher frequencies in the light.

The computational model can account for the phenotypical differences

Next, we investigated whether we could simulate the behaviour of the various genetic mouse models by only changing the resting membrane potential of the ON-CBC. The mutations in *Nyx*^{nob} and *Grm6*^{nob3} mice both affect the photoreceptor to ON-BC synapses, leading to depolarization of the ON-BCs. The *Ca*$_v$*1.4*-KO mutation, on the other hand, blocks the output of the photoreceptors also leading to depolarization of the ON-BCs. Therefore, we hypothesized that the various phenotypical differences in the three mouse models are caused by differing degrees of ON-BC depolarization. Stronger depolarization of ON-BCs leads to depolarization of A_{II} ACs, and increased oscillation frequency in both the A_{II} ACs and RGCs. We tested this hypothesis using the computational model. To change the resting membrane potential of the model ON-BC we injected a steady current into the model ON-BC.

Figure 8 gives an overview of the results for our simulations of the spontaneous activity occurring in the dark. The RGC spiking activity is shown as raster plots in Fig. 8*A* and the average spike activity of all RGCs in Fig. 8*B*. The autocorrelations of the RGC activity (Fig 8*C*) indicate oscillatory RGC firing for the *Nyx*^{nob} and *Ca*$_v$*1.4-KO* mice. In contrast to the other mouse models, the *Grm6*^{nob3} model shows no periodic bursting activity but only very high-frequency single spike activity. PSD analysis of RGC firing (Fig 8*D*) shows clear peaks at 6 and 10 Hz for the *Nyx*^{nob} and *Ca*$_v$*1.4-KO* conditions, respectively and no peak for *Grm6*^{nob3} in that frequency range. The activity of RGCs is not synchronized for either *Nyx*^{nob} or *Grm6*^{nob3}, as evidenced by the lack of any clear periodic pattern in their averaged RGC activity (Fig 8*B*). However, for *Ca*$_v$*1.4-KO* a periodic pattern is apparent, indicating synchronized firing between the RGCs. This shows that the model can reproduce the behaviour of the RGCs in the dark in the various CSNB models adequately by only changing the ON-CBC resting membrane potential by current injection.

Figure 9 shows the RGC activity for *Nyx*^{nob} and the *Grm6*^{nob3} directly after a full field light stimulus. The full field light stimulus was simulated by injecting an equal current into all A_{II} ACs. Figure 9*A* shows the raster plots of the RGCs for *Nyx*^{nob} and *Grm6*^{nob3}. No data for *Ca*$_v$*1.4-KO* in the light are presented as these retinas are not light responsive. It is clear that the RGCs oscillate in phase and that the oscillation frequency in *Nyx*^{nob} mice is higher than for *Grm6*^{nob3}. This is similar to what we found experimentally.

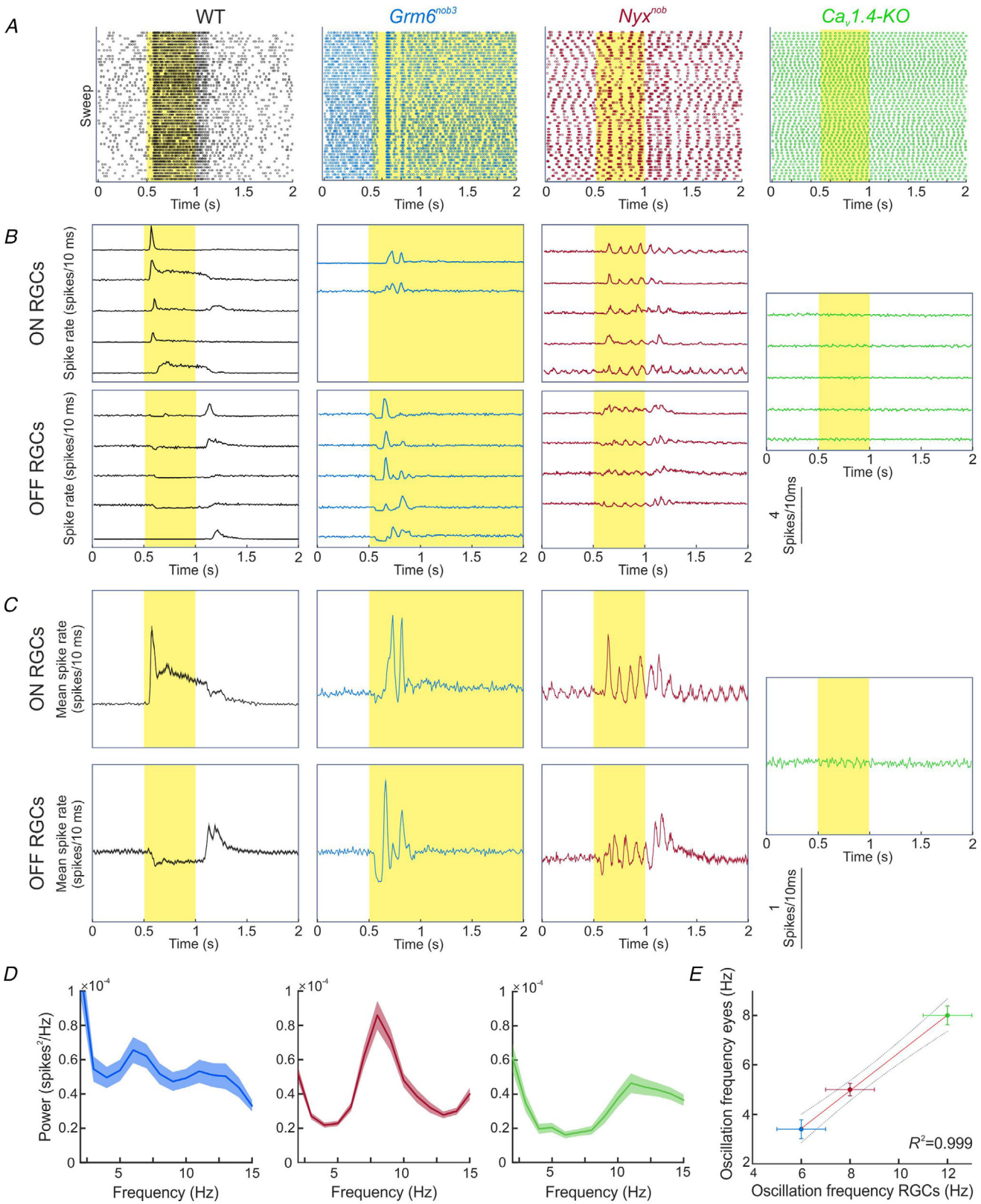

Figure 5. Comparison of the light responses of WT, *Grm6*^{nob3}, *Nyx*^{nob} and *Ca*$_v$*1.4-KO* RGCs
A, raster plots comparing the light responses of, in each case, one RGC from WT (black), *Grm6*^{nob3} (blue), *Nyx*^{nob} (red) and *Ca*$_v$*1.4-KO* (green). *B*, example light response traces showing the oscillatory activity of the four genotypes.

The *Nyx*^{nob} data were replotted from Winkelman et al. (2019). *C*, mean activity during a 500 ms/1 s light flash for the RGCs shown in *B*. *D*, mean power spectra of *Grm6*^{nob3} ($n = 17$, $N = 3$), *Nyx*^{nob} ($n = 245$, $N = 7$) and *Ca*$_v$*1.4-KO* ($n = 95$, $N = 4$) RGCs. *E*, relationship between the median RGC and eye movement oscillation frequencies for the three mouse models. The linear regression model fitted is $y = -1.16 + 0.76x$.

Discussion

In the current study, we show that in all three mouse models with mutations associated with CSNB, i.e. *Grm6*^{nob3}, *Nyx*^{nob},and *Ca*$_v$*1.4-KO* mice, RGCs and eye movements oscillate. The oscillation frequencies of the RGCs and eye movements showed a strong positive linear relationship, with each genotype displaying consistent and aligned phenotypical characteristics. First, the oscillation frequencies associated with each genotype differed, with the lowest frequencies present in *Grm6*^{nob3} mice and highest in *Ca*$_v$*1.4-KO* mice. Second, only vertical gratings induced eye movement oscillations in *Grm6*^{nob3} and *Nyx*^{nob} mice, whereas for *Ca*$_v$*1.4-KO* mice they occurred in all stimulus conditions. Third, in the dark the spontaneous firing of RGCs in *Nyx*^{nob} and *Ca*$_v$*1.4-KO* mice oscillated, but did not for *Grm6*^{nob3} mice. Fourth, light-flash stimuli led to synchronized RGC oscillations in *Nyx*^{nob} and *Grm6*^{nob3} mice, but not in *Ca*$_v$*1.4-KO* mice. Finally, in the dark *Ca*$_v$*1.4-KO* RGC firing displayed a degree of inherent synchronization that was not present for *Nyx*^{nob} and *Grm6*^{nob3}. Our modelling experiments indicate that these different outcomes may well arise from a single retinal source when taking the A_{II} ACs as a common mediator.

Similar mechanism underlying the nystagmus in the three mouse models

Can our previously proposed retinal origin of nystagmus model account of the present results (Winkelman et al., 2019)? In short, the proposed mechanism works as follows. In *Nyx*^{nob} mice A_{II} ACs are depolarized outside their normal working range, which makes them oscillate spontaneously. However, due to small input differences in the various A_{II} ACs, they all oscillate with slightly different frequencies and phases. These oscillations are transmitted to the RGCs, including the ON direction selective RGCs (ON-DSRGCs). In the dark, the signals from the ON-DSRGCs to the AOS are asynchronous and so the convergent signal generated is not large enough to induce an eye movement. However, as soon as a light stimulus occurs, the phase values of the activity of the various A_{II} ACs are reset, which synchronizes their oscillations and subsequently those of the RGCs as well. When the AOS integrates these synchronized RGC inputs, the resulting signal is large enough to induce an eye movement. In turn, this eye movement induces a new visual stimulus, which again synchronizes the retinal oscillations and the loop repeats.

What causes the differences between the phenotypes of the three mouse models?

Can our proposal account for the distinct phenotypes of each of the three CSNB mouse models displayed? These distinct features include: (1) different oscillation frequency of each CSNB model, (2) the absence of spontaneous RGC oscillations in the dark for the *Grm6*^{nob3} mice, and (3) the stimulus-independent synchronized oscillations of the RGCs in *Ca*$_v$*1.4-KO* mice?

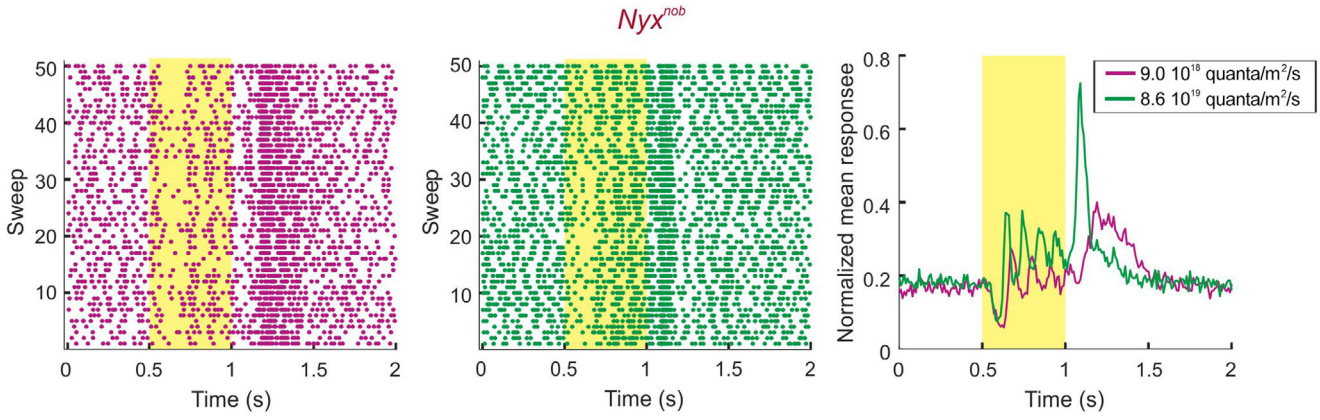

Figure 6. RGC oscillation frequency depends on light intensity
Left: raster plots of the light response of one example *Nyx*^{nob} RGC for two different light intensities. Right: mean light response of this example cell over the 100 traces showing that the oscillation frequency increases with higher light intensity.

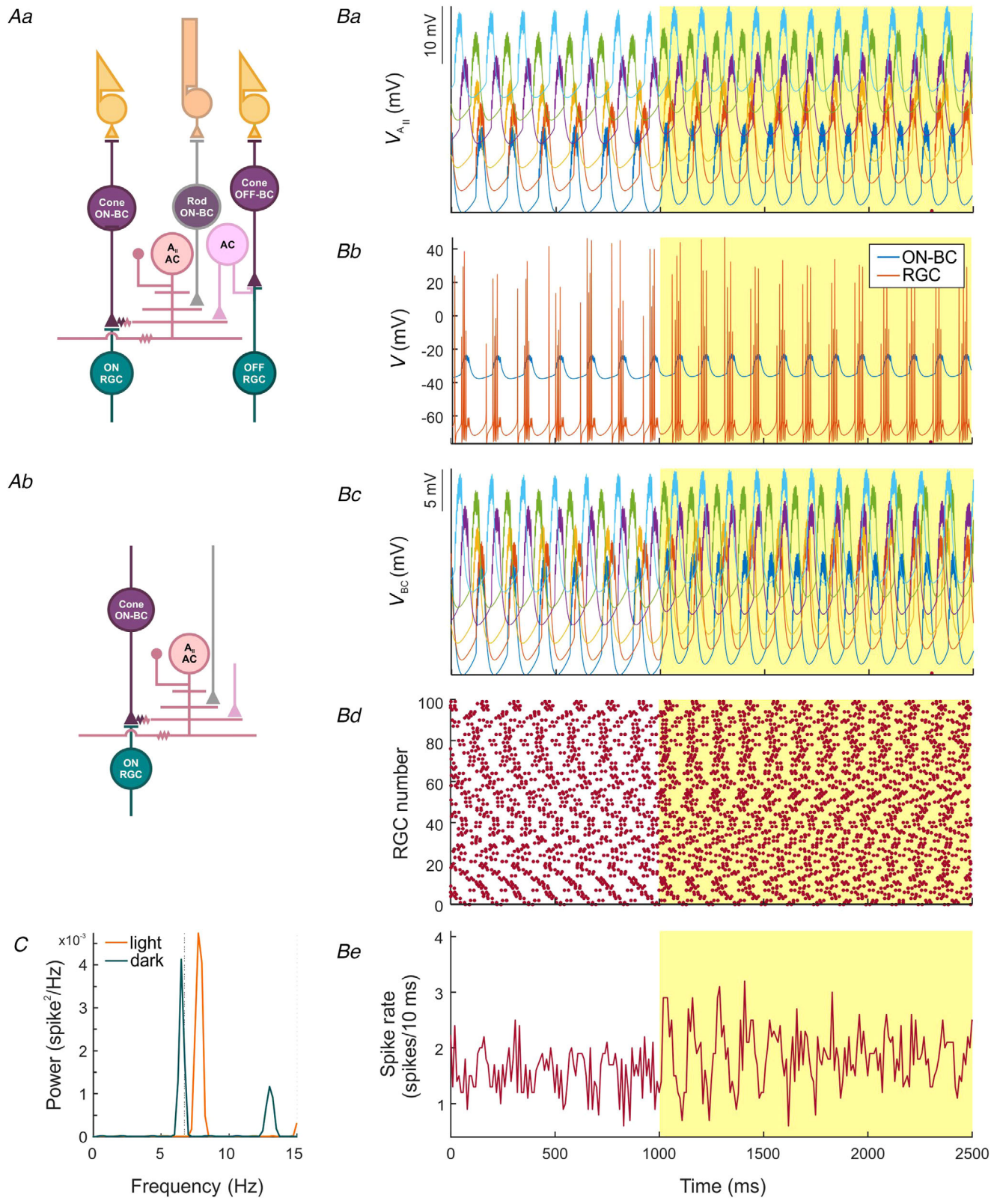

Figure 7. Overview of the model response
Aa, schematic representation of the retinal circuitry; *Ab*, schematic representation of the model. *B*, model response for *Nyx*^{nob}. *Ba*, overlay of six A_{II} ACs. *Bb*, overlay of a single BC and RGC. *Bc*, overlay of six BCs. *Bd*, raster plot of all RGCs. *Be*, average spiking activity. *C*, averaged power spectral density of all RGC activity.

Differences in oscillation frequencies. The A_{II} AC oscillation frequency depends on its membrane potential; the more depolarized A_{II} ACs are, the higher is the oscillation frequency (Choi et al., 2014). This suggests that the A_{II} AC membrane potential in the various CSNB mouse models is more depolarized than in WT, with *$Ca_v1.4$-KO* A_{II} ACs being the most depolarized and *Grm6^{nob3}* the least. A_{II} ACs are ON cells meaning that they depolarize with a reduction of glutamate release by the photoreceptors either via a direct ON-BC input or via a crossover inhibitory input from the OFF-BC pathway. Blocking all glutamate release from the photoreceptors, as is that case in the *$Ca_v1.4$-KO* mice, would lead to a strong depolarization of the A_{II} ACs and thus a high oscillation frequency. Indeed, the oscillation frequency in the *$Ca_v1.4$-KO* animals is highest. In *Nyx^{nob}* animals the A_{II} ACs seem to be less depolarized, because the crossover inhibition from the OFF-BCs is still intact, which keeps the A_{II} ACs somewhat more hyperpolarized compared to the *$Ca_v1.4$-KO* mice. Our results also suggest that the A_{II} ACs in *Grm6^{nob3}* are less depolarized than they are in *Nyx^{nob}*. We can only speculate why this may be so, but presumably the absence of the mGluR6 receptor affects the synapse differently than does the absence of the scaffolding protein nyctalopin. Unfortunately, the available literature regarding the exact resting membrane potentials of ON-BCs in the CSNB mouse models is contradictory (Ishii et al., 2009; O'Connor et al., 2006; Tagawa et al., 1999; Xu et al., 2012). However, following the arguments of Ishii et al. (2009), O'Conner et al. (2006) and Tagawa et al. (1999), it seems likely that ON-bipolar cells in the CSNB mouse models studied are constitutively depolarized.

Why are *Grm6^{nob3}* RGCs not oscillating spontaneously in the dark? We propose that in the dark the *Grm6^{nob3}* A_{II} ACs are resting at potentials just below that required to initiate spontaneous membrane potential oscillations. However, when stimulated with light they depolarize further and start to oscillate. This could explain why we and others (Takeuchi et al., 2018) find so few oscillating RGCs in the *Grm6^{nob3}* retina compared with the other CSNB mouse models. One prediction of our proposed mechanism is that the oscillation frequency of the RGCs depends on the light intensity. Indeed, the oscillation

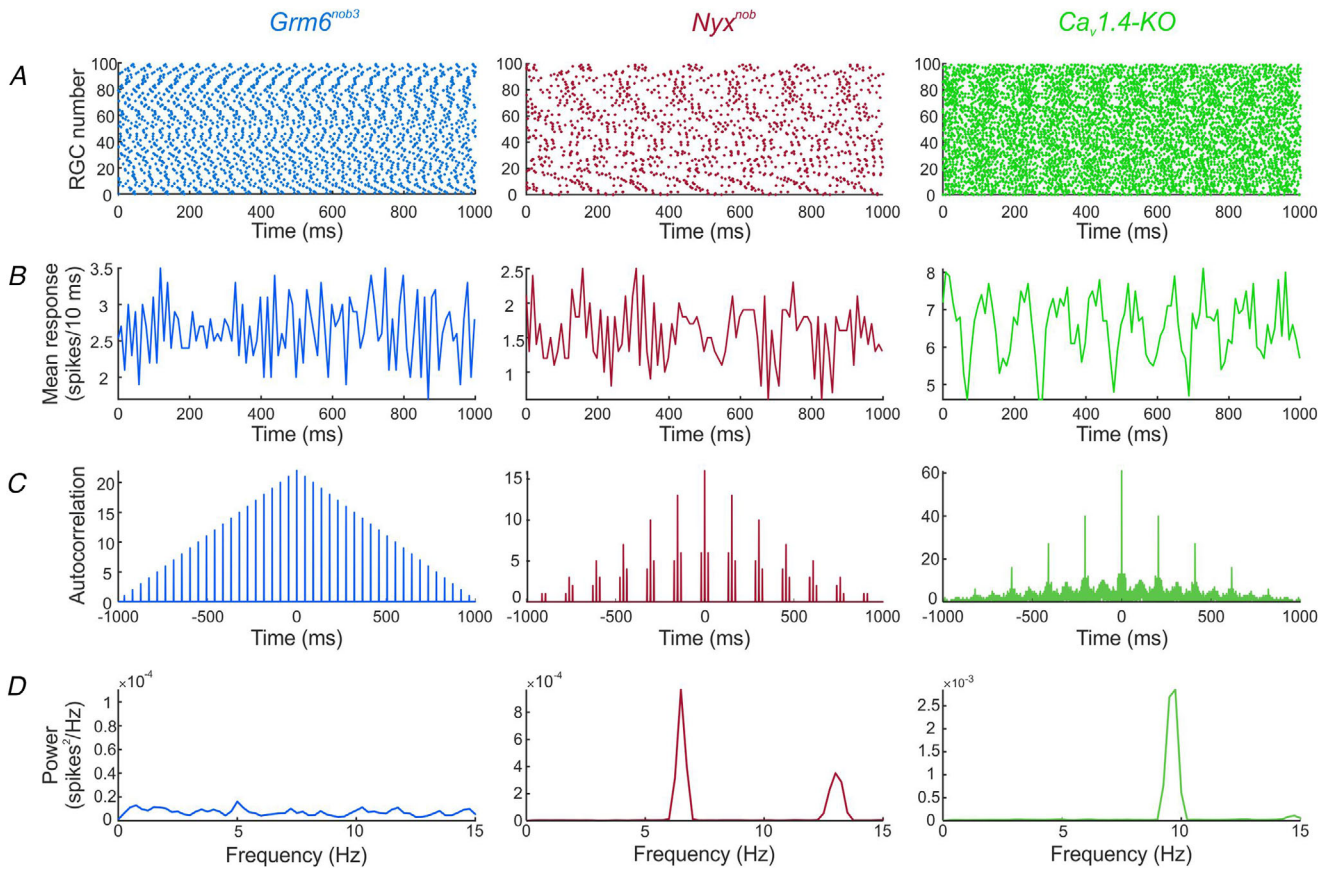

Figure 8. Simulated RGC activity in the dark for the three different CSNB mouse models
A, raster plots of RGCs. *B*, average spiking activity. *C*, cross-correlation of RGC activity. *D*, power spectral density plots.

frequency in the *Nyx*^{nob} RGC increases with a higher light intensity and therefore the membrane potential of the A_{II} AC.

Why do RGCs and eyes in the *Ca$_v$1.4-KO* mice oscillate under all stimulus conditions? *Ca$_v$1.4-KO* mice are blind and our results indicate their A_{II} ACs are strongly depolarized and oscillate with a degree of inherent synchronization. This suggests that the coupling strength of A_{II} ACs is higher in the *Ca$_v$1.4-KO* retinas than in the other CSNB mouse models. The electrical coupling strength of neurons depends on the ratio of the gap junction conductance and the input conductance of the coupled neurons.

In *Ca$_v$1.4-KO*, crossover inhibition from the OFF pathway to the A_{II} ACs is also impaired and thus the associated inhibitory conductance will be closed. Accordingly, the input resistance of the A_{II} ACs in *Ca$_v$1.4-KO* is likely to be higher than for the other CSNB mouse models. The reciprocal decrease in input conductance shifts the ratio towards the gap junction conductance, increasing the electrical coupling strength between coupled A_{II} ACs. This increase in coupling between oscillating A_{II} ACs in *Ca$_v$1.4-KO* enables the occurrence of an entrained oscillation state across the A_{II} AC network.

Model simulations show that the different oscillation frequencies in the various mutations originate in ON-BC membrane potential differences

We constructed a model consisting of a grid of hexagonally arranged units consisting of a ON-CBC that is electrically coupled to an A_{II} AC and synaptically to an ON-RGC (Fig. 7*Ab*). To account for the slight differences in oscillation frequency of the RGCs within

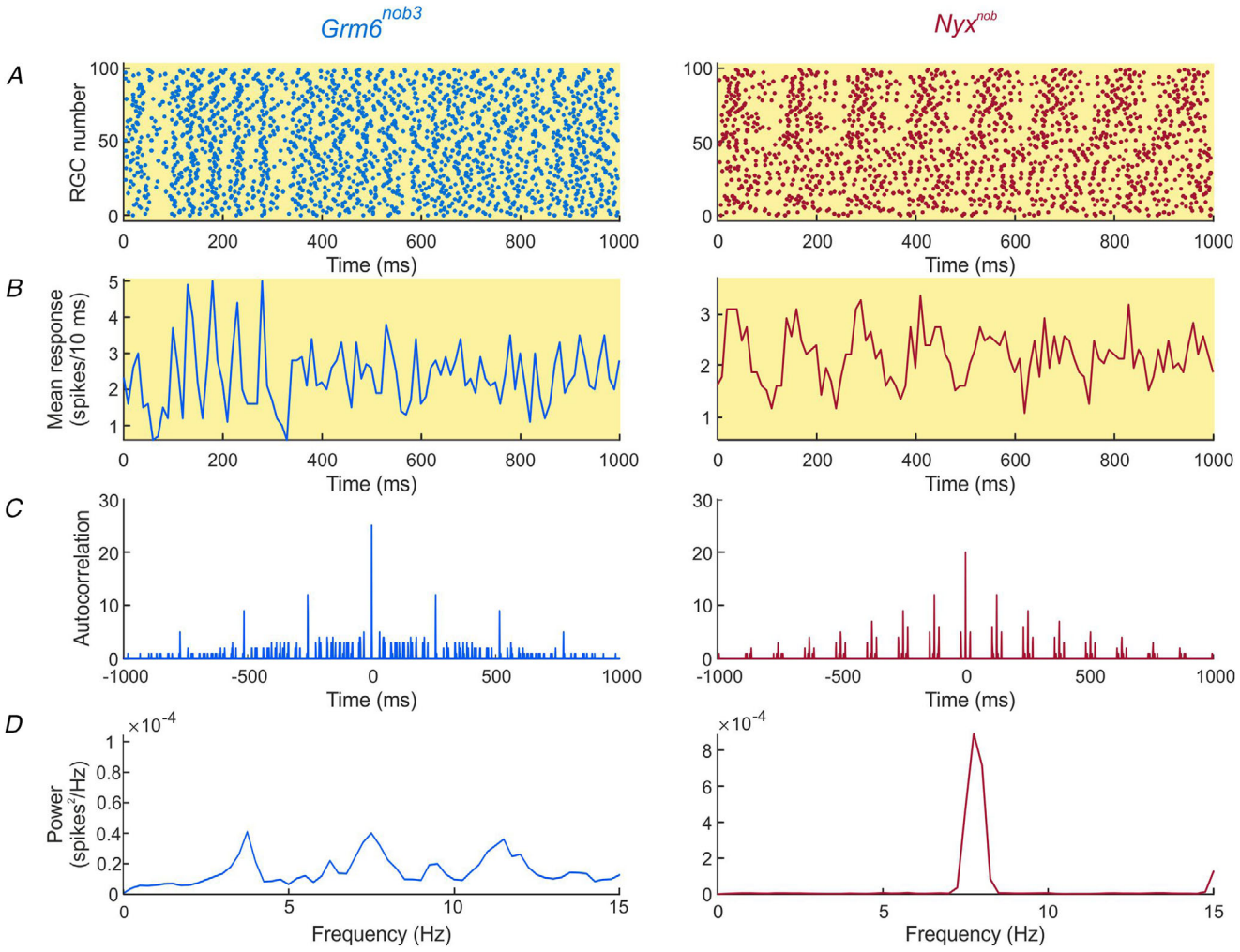

Figure 9. Simulated RGC activity after a light stimulus for *Grm6^{nob3}* (blue) and *Nyx^{nob}* (red) mice
A, raster plots of the spiking activity of RGCs. *B*, average spiking activity for the cells shown in *A*. *C*, cross-correlation of RGC activity. *D*, power spectral density plots.

each genotype, each A_{II} AC received a slightly different bias current such that their resting membrane potentials differed slightly. First, we tested whether it is possible to simulate the phenotypical differences in the spontaneous oscillatory behaviour of RGCs in the dark for the three mouse models. Variable amounts of current were injected into the ON-CBCs to manipulate their resting membrane potential. The resting membrane potential was depolarized the least to simulate the *Grm6*^{nob3} condition and the most for the *Ca$_v$1.4-KO* simulation. Under these settings the *Grm6*^{nob3} RGCs did not oscillate while the *Nyx*^{nob} and *Ca$_v$1.4-KO* RGCs oscillated at 6 and 10 Hz respectively. Hence, by manipulating a single parameter, the model reproduced the experimentally observed RGC behaviour in the dark.

Next, we tested if the difference in resting membrane potential of ON-BCs could also reproduce the phenotypical differences in the RGC light flash responses of the various mouse models. As the experiment data show that light flash stimuli synchronize the RGC oscillations (Figs 5 and 6; Winkelman et al., 2019), we first confirmed that the model could replicate this behaviour. Figure 7*B* shows the activity of the various model cells before, and during, a stimulated light stimulus. Before the stimulus, the A_{II} ACs are spontaneously oscillating independently because they are each at a different resting membrane potential and consequently the averaged activity of the RGCs shows no oscillations (Fig. 7*Be*, $t < 1000$ ms). As the ON pathway is not light sensitive in CSNB, we assumed A_{II} AC light responses were generated by input from an inhibitory AC driven by OFF-BCs, which we simulated as a current injection. Injecting an equal current pulse into all A_{II} ACs phase resets their own oscillations, and consequently leads to synchronized RGC activity. Now the mean activity of the RCS showed clear oscillations (Fig. 7*Be*, 1000 ms $\leq t \leq$ 1500 ms). Furthermore, the oscillations in the RGC mean activity diminished over time (Fig. 7*Be*, $t >$ 1500ms) indicating this synchronization is gradually lost. This occurs because though A_{II} AC oscillations are initially in phase, their individual oscillation frequencies are still different and over time this leads to phase differences and loss of synchrony. This behaviour matches the experimental data.

Finally, we simulated the response to a light flash in the model phenotypes for *Nyx*^{nob} and *Grm6*^{nob3} (Fig. 9). This simulation replicated several key characteristics observed in the experimental data (Fig. 5). The *Grm6*^{nob3} RGCs showed oscillatory firing during the light flash simulation, which dampened out sooner and oscillated at a lower frequency compared to the *Nyx*^{nob} RGCs. Thus, the model indicates again that the phenotypical differences we observed between the different mouse models can be accounted for by only depolarizing the membrane potential of the ON-BCs.

Alternative mechanisms leading to RGC oscillations

Our data, both here and in earlier publications (Winkelman et al., 2019), and modelling work support our proposed role of A_{II} ACs as the driver of the RGC oscillations we observe in CSNB mouse models. However, alternative mechanisms may also account for the RGC oscillations. In the following section we discuss possible alternatives and issues, as well as our rational for why our A_{II} AC proposal is still the most parsimonious explanation.

Could each mutation have a separate and distinct working mechanism for the induction of nystagmus? Since the genes studied are ON-BC- (*Nyx* and *Grm6*) or photoreceptor-specific (*Ca$_v$1.4*), alternative mechanisms should be based on a non-functional modulation of the TRPM1 channels, as this is the first common target in the system in all the mouse models. This strongly limits the number of alternative mechanisms leading to oscillating RGCs and consequently the nystagmus. Changes in activation of the TRPM1 channel lead to changes in the membrane potential of the ON-BC. Having separate mechanisms for the various mutations would imply that subtle changes of the ON-BC membrane potential would activate vastly different pathways. There is no evidence for such a demarcation point in the ON-BC responses to the RGCs. Furthermore, such a system would be very instable. It is therefore highly unlikely that the various mutations work via different mechanisms.

Could there be more than one oscillator in the retina? What would these other oscillators be? The oscillations in both the retinal degeneration (rd) mouse models and the CSNB mouse models seem to be widespread over the various retinal layers, occurring in many ACs and BCs, making it unlikely that they originate in the RGCs themselves. Furthermore, to the best of our knowledge, there is no evidence, either functional or morphological, to suggest that RGCs feed back into the A_{II} AC system. The most likely site of the oscillators would be the ACs or networks that involve ACs. Although we cannot exclude that other AC types are driving the oscillations as well, our data are consistent with A_{II} ACs as the single origin of the oscillation.

Based on pharmacological experiments, Tu et al. (2016) suggested that the oscillations in the RGCs are driven by two distinct oscillators in the retina. Our work, on the other hand, suggests that A_{II} ACs form a population of oscillators with slightly different oscillation frequencies that drive the RGC oscillations. In the dark the A_{II} ACs oscillate asynchronously, all with their own frequency. Light stimulation can synchronize the A_{II} ACs, which is a property of the ON-BC – A_{II} AC network. The synchronized activity of the A_{II} ACs is

then transmitted to the ON- and OFF-BCs via two pharmacologically different pathways. The pathway to the ON-CBCs is routed via gap junctions to the ON-CBC terminal, which also receives strong GABAergic inhibition (Marc et al., 2014). The pathway to the OFF-BCs runs via glycinergic input to the OFF-BCs. So, some pharmacological experiments may block the output of the A_{II} ACs to the ON-pathway while others may block the output to the OFF-pathway. Thus, the pharmacological experiments of Tu et al. (2016) can also be interpreted as nicely revealing the difference in pharmacology of the output pathways of the A_{II} ACs and not per se as evidence for more than one oscillator.

Based on these considerations, the blocking/Cx36-knockout experiments we performed previously in *Nyx*^{nob} mice (Winkelman et al., 2019) and the modelling work presented in this paper, we propose that the A_{II} ACs are exclusively the oscillators that drive the nystagmus. Consistently, by solely changing the membrane potential of the ON-BCs in our model while keeping all other parameters the same, we can account for the *Nyx*^{nob}, *Grm6*$^{-/-}$ and the *Ca*$_v$*1.4-KO* results.

Causal relationship between RGCs and eye movement oscillations

One hypothesis for the cause of nystagmus is a mal-adapted oscillating OKN loop (see Kamermans et al., 2023 for a discussion). Opening such a loop should stop oscillation throughout the loop and abolish nystagmus. Recently, we presented evidence that nystagmus in CSNB is not caused by such an oscillating loop (Winkelman et al., 2019), but instead by intrinsic retinal oscillations. The present paper adds to that conclusion in a rather direct way.

Consistent with previous reports (Michalakis et al., 2014), our results indicate *Ca*$_v$*1.4-KO* mice are blind and as such their visual impairment is greater than is found in human patients with similar mutations. Since the photoreceptor output is absent with this mutation, it is interesting to compare results of the present study with those of the DNQX + D-AP5 experiments in *Nyx*^{nob} mice we described earlier (Winkelman et al., 2019). This drug cocktail blocks all RGC inputs. In that paper we showed that applying this drug cocktail abolished all RGC oscillations in the isolated retina. When this cocktail was injected into the eyes of *Nyx*^{nob} mice, eye movement oscillations stopped. This result is consistent with our hypothesis of a retinal origin of nystagmus in CSNB. However, this experiment does not per se discriminate between two possible conditions. The result could have occurred because blocking RGC inputs opened the oscillating OKR loop or because a retinal oscillator was silenced.

For the *Ca*$_v$*1.4-KO* mice, since the photoreceptor output is blocked, their mutation also opens the OKR loop but now at the site of the photoreceptors, while leaving the RGC inputs intact. Hence, the output from oscillating A_{II} ACs is not blocked and still reaches the RGCs. The finding that these mice still have oscillating eye movements shows that the oscillating A_{II} ACs are driving the nystagmus. Thus, although we cannot exclude some secondary modifications of the eye movement system downstream, these experiments confirm the retinal origin of the nystagmus in the CSNB mouse models and a causal relationshipn between RGC and eye movement oscillations.

Differences in RGC and eye movement oscillation frequency

While there is a clear linear relationship between the RGC and eye movement oscillations, the RGC oscillation frequencies are slightly higher than the frequencies for eye movements. This difference is probably caused by the different physiological conditions of the *in vitro* and *in vivo* experiments. Many factors such as pH, the composition of the external solution and potential retinal damage during the dissection may have influenced the RGC oscillations during the *in vitro* electrophysiological recordings. Differences between *in vivo* and *in vitro* conditions have been reported previously by other research groups as well (Belle et al., 2018; Meijer et al., 1997).

Mechanism potentially underlying other forms of nystagmus

The retinal mechanism we propose to cause nystagmus is probably not only limited to CSNB since any condition that can depolarize A_{II} ACs beyond their normal working range will lead them to oscillate, possibly introducing nystagmus. Interestingly, a specific mutation in Munc 18-1 leads also to nystagmus (Li et al., 2020). Munc 18-1 is involved in the docking of synaptic vesicles to the membrane. It does so by binding with syntaxin. In the photoreceptor synaptic terminal Munc 18-1 binds to syntaxin 3B (Curtis et al., 2010). The mutation leading to nystagmus enhances the binding of Munc 18-1 with syntaxin 3B (Li et al., 2020). This mutation probably leads to reduced glutamate release by the photoreceptors resulting in depolarization of the A_{II} ACs, which in turn will start to oscillate and eventually lead to nystagmus. This example illustrates that it is essential to investigate whether novel genes implicated in nystagmus may have affected the A_{II} AC membrane potential and in that way have induced nystagmus. This knowledge will allow us

to limit future therapeutic strategies to one common approach.

References

Attivissimo, F., Savino, M., & Trotta, A. (2000). A study on nonlinear averagings to perform the characterization of power spectral density estimation algorithms. *IEEE Transactions on Instrumentation and Measurement*, **49**(5), 1036–1042.

Belle, A. M., Enright, H. A., Sales, A. P., Kulp, K., Osburn, J., Kuhn, E. A., Fischer, N. O., & Wheeler, E. K. (2018). Evaluation of in vitro neuronal platforms as surrogates for in vivo whole brain systems. *Scientific Reports*, **8**(1), 10820.

Bijveld, M. M. C., Florijn, R. J., Bergen, A. A. B., van den Born, L. I., Kamermans, M., Prick, L., Riemslag, F. C. C., van Schooneveld, M. J., Kappers, A. M. L., & van Genderen, M. M. (2013). Genotype and phenotype of 101 dutch patients with congenital stationary night blindness. *Ophthalmology*, **120**(10), 2072–2081.

Brainard, D. H. (1997). The psychophysics toolbox. *Spatial Vision*, **10**(4), 433–436.

Cao, Y., Masuho, I., Okawa, H., Xie, K., Asami, J., Kammermeier, P. J., Maddox, D. M., Furukawa, T., Inoue, T., Sampath, A. P., & Martemyanov, K. A. (2009). Retina-specific GTPase accelerator RGS11/Gβ5S/R9AP is a constitutive heterotrimer selectively targeted to mGluR6 in ON-bipolar neurons. *The Journal of Neuroscience*, **29**(29), 9301–9313.

Cao, Y., Posokhova, E., & Martemyanov, K. A. (2011). TRPM1 forms complexes with nyctalopin *in vivo* and accumulates in postsynaptic compartment of ON-bipolar neurons in mGluR6-dependent manner. *The Journal of Neuroscience*, **31**(32), 11521–11526.

Choi, H., Zhang, L., Cembrowski, M. S., Sabottke, C. F., Markowitz, A. L., Butts, D. A., Kath, W. L., Singer, J. H., & Riecke, H. (2014). Intrinsic bursting of AII amacrine cells underlies oscillations in the rd1 mouse retina. *Journal of Neurophysiology*, **112**(6), 1491–1504.

Curtis, L., Datta, P., Liu, X., Bogdanova, N., Heidelberger, R., & Janz, R. (2010). Syntaxin 3B is essential for the exocytosis of synaptic vesicles in ribbon synapses of the retina. *Neuroscience*, **166**(3), 832–841.

Gregg, R. G., Kamermans, M., Klooster, J., Lukasiewicz, P. D., Peachey, N. S., Vessey, K. A., & McCall, M. A. (2007). Nyctalopin expression in retinal bipolar cells restores visual function in a mouse model of complete X-linked congenital stationary night blindness. *Journal of Neurophysiology*, **98**(5), 3023–3033.

Gregg, R. G., Mukhopadhyay, S., Candille, S. I., Ball, S. L., Pardue, M. T., McCall, M. A., & Peachey, N. S. (2003). Identification of the gene and the mutation responsible for the mouse nob phenotype. *Investigative Ophthalmology & Visual Science*, **44**(1), 378.

Gregg, R. G., Ray, T. A., Hasan, N., McCall, M. A., & Peachey, N. S. (2014). Interdependence among members of the mGluR6 G-protein mediated signalplex of retinal depolarizing bipolar cells. *G protein signaling mechanisms in the retina*, (pp. 67–79). Springer, New York, NY.

Hölzel, M.-B., Howlett, M. H. C., & Kamermans, M. (2022). Receptive field sizes of Nyx(nob) mouse retinal ganglion cells. *International Journal of Molecular Sciences*, **23**(6), 3202.

Ishii, M., Morigiwa, K., Takao, M., Nakanishi, S., Fukuda, Y., Mimura, O., & Tsukamoto, Y. (2009). Ectopic synaptic ribbons in dendrites of mouse retinal ON- and OFF-bipolar cells. *Cell and Tissue Research*, **338**(3), 355–375.

Kamermans, M., Winkelman, B. H. J., Hölzel, M.-B., Howlett, M. H. C., Kamermans, W., Simonsz, H. J., & de Zeeuw, C. I. (2023). A retinal origin of nystagmus—a perspective. *Frontiers in Ophthalmology*, **3**. https://doi.org/10.3389/fopht.2023.1186280

Koike, C., Obara, T., Uriu, Y., Numata, T., Sanuki, R., Miyata, K., Koyasu, T., Ueno, S., Funabiki, K., Tani, A., Ueda, H., Kondo, M., Mori, Y., Tachibana, M., & Furukawa, T. (2010). TRPM1 is a component of the retinal ON bipolar cell transduction channel in the mGluR6 cascade. *Proceedings of the National Academy of Sciences*, **107**(1), 332–337.

Kreuz, T., Mulansky, M., & Bozanic, N. (2015). SPIKY: A graphical user interface for monitoring spike train synchrony. *Journal of Neurophysiology*, **113**(9), 3432–3445.

Li, Y., Jiang, L., Wang, L., Wang, C., Liu, C., Guo, A., Liu, M., Zhang, L., Ma, C., Zhang, X., Gao, S., & Liu, J. Y. (2020). p.His16Arg of STXBP1 (MUNC18-1) associated with syntaxin 3B causes autosomal dominant congenital nystagmus. *Frontiers in Cell and Developmental Biology*, **8**, 591781.

Maddox, D. M., Vessey, K. A., Yarbrough, G. L., Invergo, B. M., Cantrell, D. R., Inayat, S., Balannik, V., Hicks, W. L., Hawes, N. L., Byers, S., Smith, R. S., Hurd, R., Howell, D., Gregg, R. G., Chang, B., Naggert, J. K., Troy, J. B., Pinto, L. H., Nishina, P. M., & McCall, M. A. (2008). Allelic variance between GRM6 mutants, Grm6nob3 and Grm6nob4 results in differences in retinal ganglion cell visual responses. In *Journal of Physiology*, **586**(18), 4409–4424,

Marc, R. E., Anderson, J. R., Jones, B. W., Sigulinsky, C. L., & Lauritzen, J. S. (2014). The AII amacrine cell connectome: a dense network hub. *Frontiers in Neural Circuits*, **8**, 104.

Martemyanov, K. A., & Sampath, A. P. (2017). The transduction cascade in retinal ON-bipolar cells: Signal processing and disease. *Annual review of vision science*, **3**(1), 25–51.

Masu, M., Iwakabe, H., Tagawa, Y., Miyoshi, T., Yamashita, M., Fukuda, Y., Sasaki, H., Hiroi, K., Nakamura, Y., Shigemoto, R., Takada, M., Nakamura, K., Nakao, K., Katsuki, M., & Nakanishi, S. (1995). Specific deficit of the ON response in visual transmission by targeted disruption of the mGIuR6 gene. *Cell*, **80**(5), 757–765.

Meijer, J. H., Schaap, J., Watanabe, K., & Albus, H. (1997). Multiunit activity recordings in the suprachiasmatic nuclei: In vivo versus in vitro models. *Brain Research*, **753**(2), 322–327.

Michalakis, S., Shaltiel, L., Sothilingam, V., Koch, S., Schludi, V., Krause, S., Zeitz, C., Audo, I., Lancelot, M. E., Hamel, C., Meunier, I., Preising, M. N., Friedburg, C., Lorenz, B., Zabouri, N., Haverkamp, S., Garcia Garrido, M., Tanimoto, N., Seeliger, M. W., … Wahl-Schott C. A. (2014). Mosaic synaptopathy and functional defects in Cav1.4 heterozygous mice and human carriers of CSNB2. *Human Molecular Genetics*, **23**(6), 1538–1550.

Morgans, C. W., Zhang, J., Jeffrey, B. G., Nelson, S. M., Burke, N. S., Duvoisin, R. M., & Brown, R. L. (2009). TRPM1 is required for the depolarizing light response in retinal ON-bipolar cells. *Proceedings of the National Academy of Sciences*, **106**(45), 19174–19178.

O'Connor, E., Allen, L. E., Bradshaw, K., Boylan, J., Moore, A. T., & Trump, D. (2006). Congenital stationary night blindness associated with mutations in GRM6 encoding glutamate receptor MGluR6 [7]. *British Journal of Ophthalmology*, **90**(5), 653–654.

Optican, L. M., & Zee, D. S. (1984). A hypothetical explanation of congenital nystagmus. *Biological Cybernetics*, **50**(2), 119–134.

Pardue, M. T., McCall, M. A., LaVail, M. M., Gregg, R. G., & Peachey, N. S. (1998). A naturally occurring mouse model of X-linked congenital stationary night blindness. *Investigative Ophthalmology & Visual Science*, **39**(12), 2443–2449

Pearring, J. N., Bojang, P., Shen, Y., Koike, C., Furukawa, T., Nawy, S., & Gregg, R. G. (2011). A role for nyctalopin, a small leucine-rich repeat protein, in localizing the TRP melastatin 1 channel to retinal depolarizing bipolar cell dendrites. *Journal of Neuroscience*, **31**(27), 10060–10066.

Pieh, C., Simonsz-Toth, B., & Gottlob, I. (2008). Nystagmus characteristics in congenital stationary night blindness (CSNB). *British Journal of Ophthalmology*, **92**(2), 236–240.

Pintelon, R., Schoukens, J., & Renneboog, J. (1988). The geometric mean of power (amplitude) spectra has a much smaller bias than the classical arithmetic (RMS) averaging. *IEEE Transactions on Instrumentation and Measurement*, **37**(2), 213–218.

Quiroga, R. Q., Nadasdy, Z., & Ben-Shaul, Y. (2004). Unsupervised spike detection and sorting with wavelets and superparamagnetic clustering. *Neural Computation*, **16**(8), 1661–1687.

Ray, T. A., Heath, K. M., Hasan, N., Noel, J. M., Samuels, I. S., Martemyanov, K. A., Peachey, N. S., McCall, M. A., & Gregg, R. G. (2014). GPR179 is required for high sensitivity of the mGluR6 signaling cascade in depolarizing bipolar cells. *The Journal of Neuroscience*, **34**(18), 6334–6343.

Satuvuori, E., Mulansky, M., Bozanic, N., Malvestio, I., Zeldenrust, F., Lenk, K., & Kreuz, T. (2017). Measures of spike train synchrony for data with multiple time scales. *Journal of Neuroscience Methods*, **287**, 25–38.

Schmitz, Y., & Witkovsky, P. (1997). Dependence of photoreceptor glutamate release on a dihydropyridine- sensitive calcium channel. *Neuroscience*, **78**(4), 1209–1216.

Shen, Y., Heimel, J. A., Kamermans, M., Peachey, N. S., Gregg, R. G., & Nawy, S. (2009). A transient receptor potential-like channel mediates synaptic transmission in rod bipolar cells. *Journal of Neuroscience*, **29**(19), 6088–6093.

Sigulinsky, C. L., Anderson, J. R., Kerzner, E., Rapp, C. N., Pfeiffer, R. L., Rodman, T. M., Emrich, D. P., Rapp, K. D., Nelson, N. T., Lauritzen, J. S., Meyer, M., Marc, R. E., & Jones, B. W. (2020). Network architecture of gap junctional coupling among parallel processing channels in the mammalian retina. *The Journal of Neuroscience*, **40**(23), 4483–4511.

Specht, D., Wu, S.-B., Turner, P., Dearden, P., Koentgen, F., Wolfrum, U., Maw, M., Brandsta¨tter, J. H., & tom Dieck, S. (2009). Effects of presynaptic mutations on a postsynaptic cacna1s calcium channel colocalized with mglur6 at mouse photoreceptor ribbon synapses. *Investigative Opthalmology & Visual Science*, **50**(2), 505–515.

Stahl, J. S. (2002). Calcium channelopathy mutants and their role in ocular motor research. *Annals of the New York Academy of Sciences*, **956**(1), 64–74.

Stahl, J. S., van Alphen, A. M., & De Zeeuw, C. I. (2000). A comparison of video and magnetic search coil recordings of mouse eye movements. *Journal of Neuroscience Methods*, **99**(1–2), 101–110.

Stahl, J. S., James, R. A., Oommen, B. S., Hoebeek, F. E., & De Zeeuw, C. I. (2006). Eye movements of the murine P/Q calcium channel mutant tottering, and the impact of aging. *Journal of Neurophysiology*, **95**(3), 1588–1607.

Tagawa, Y., Sawai, H., Ueda, Y., Tauchi, M., & Nakanishi, S. (1999). Immunohistological studies of metabotropic glutamate receptor subtype 6-deficient mice show no abnormality of retinal cell organization and ganglion cell maturation. *Journal of Neuroscience*, **19**(7), 2568–2579.

Takeuchi, H., Horie, S., Moritoh, S., Matsushima, H., Hori, T., Kimori, Y., Kitano, K., Tsubo, Y., Tachibana, M., & Koike, C. (2018). Different activity patterns in retinal ganglion cells of TRPM1 and mGluR6 knockout mice. *BioMed research international*, **2018**, 1–6.

Tu, H.-Y., Chen, Y.-J., McQuiston, A. R., Chiao, C.-C., & Chen, C.-K. (2016). A novel retinal oscillation mechanism in an autosomal dominant photoreceptor degeneration mouse model. *Frontiers in Cell Neuroscience*, **9**, 513.

Usui, S., Ishihaiza, A., Kamiyama, Y., & Ishii, H. (1996). Ionic current model of bipolar cells in the lower vertebrate retina. *Vision Research*, **36**(24), 4069–4076.

Winkelman, B. H. J., Howlett, M. H. C., Hölzel, M. B., Joling, C., Fransen, K. H., Pangeni, G., Kamermans, S., Sakuta, H., Noda, M., Simonsz, H. J., McCall, M. A., De Zeeuw, C. I., & Kamermans, M. (2019). Nystagmus in patients with congenital stationary night blindness (CSNB) originates from synchronously firing retinal ganglion cells. *PLoS Biology*, **17**(9), e3000174.

Xu, Y., Dhingra, A., Fina, M. E., Koike, C., Furukawa, T., & Vardi, N. (2012). mGluR6 deletion renders the TRPM1 channel in retina inactive. *Journal of Neurophysiology*, **107**(3), 948–957.

Yonehara, K., Ishikane, H., Sakuta, H., Shintani, T., Nakamura-Yonehara, K., Kamiji, N. L., Usui, S., & Noda, M. (2009). Identification of retinal ganglion cells and their projections involved in central transmission of information about upward and downward image motion. *PLoS ONE*, **4**(1), e4320.

Zeitz, C., Robson, A. G., & Audo, I. (2015). Congenital stationary night blindness: An analysis and update of genotype-phenotype correlations and pathogenic mechanisms. *Progress in Retinal and Eye Research*, **45**, 58–110.

Additional information

Data availability statement

All original experimental data from which graphical is generated is archived (https://figshare.com/account/home#/projects/183604) and fully available. The matlab code of the model is available upon reasonable request.

Competing interests

The authors declare no conflicts of interest.

Author contributions

Conceptualization: M.B.H., M.H., B.H.W., W.K. and M.K. Methodology: M.B.H., M.H., B.H.W. and W.K. Data curation: M.B.H., M.H., B.H.W., W.K. and M.K. Formal analysis: M.B.H., B.H.W., M.H. and W.K. Funding acquisition: C.I.D.Z. and M.K. Investigation: M.B.H., M.H., B.H.W., W.K. and M.K. Project administration: M.K. Software: M.H., B.H.W. and W.K. Supervision: C.I.D.Z. and M.K. writing – original draft preparation: M.B.H. writing – review and editing: M.B.H., M.H., B.H.W., W.K., C.I.D.Z. and M.K. All authors have read and agreed to the published version of the manuscript.

Funding

This research was funded by EU-Horizon 2020, via the SwitchBoard grant, a grant from the friends foundation of the Netherlands Institute for neuroscience, by Uitzicht grants UT2016-13 and UT 2020-14, a generous donor via the Friends of the Netherlands Institute of Neuroscience Foundation, the Netherlands Organization for Scientific Research (NWO-ALW 824.02.001), the Dutch Organization for Medical Sciences (ZonMW 91120067), Medical Neuro-Delta (MD 01092019−31082023), INTENSE LSH-NWO (TTW/00798883), ERC-adv (GA-294775) and ERC-POC (nos. 737619 and 768914), and the NIN Vriendenfonds for Albinism as well as the Dutch NWO Gravitation Program (DBI2).

Acknowledgements

The authors would like to thank Cynthia Geelen for genotyping the mice.

Keywords

A_{II} amacrine cells, $Ca_v1.4$-KO, congenital nystagmus, CSNB, eye movements, *Grm6*^{nob3}, Nyx^{nob}, retina, retinal ganglion cells

Supporting information

Additional supporting information can be found online in the Supporting Information section at the end of the HTML view of the article. Supporting information files available:

Statistical Summary Document
Peer Review History